Available online at www.sciencedirect.com

ScienceDirect

Geochimica et Cosmochimica Acta 213 (2017) 553–573

Geochimica et Cosmochimica Acta

www.elsevier.com/locate/gca

Characterisation of Fe-bearing particles and colloids in the Lena River basin, NE Russia

Catherine Hirst [a,b,c,*], Per S. Andersson [a], Samuel Shaw [d], Ian T. Burke [e], Liselott Kutscher [a,b,c], Melissa J. Murphy [f], Trofim Maximov [g,h], Oleg S. Pokrovsky [i,j], Carl-Magnus Mörth [b,c], Don Porcelli [f]

[a] Department of Geosciences, Swedish Museum of Natural History, 104 05 Stockholm, Sweden
[b] Department of Geological Sciences, Stockholm University, 10 691 Stockholm, Sweden
[c] Bolin Centre for Climate Research, Stockholm University, 10 691 Stockholm, Sweden
[d] School of Earth and Environmental Sciences, University of Manchester, M13 9PL Manchester, UK
[e] School of Earth and Environment, University of Leeds, LS2 9JT Leeds, UK
[f] Department of Earth Sciences, Oxford University, OX1 3AN Oxford, UK
[g] Institute for Biological Problems of the Cryolithozone, Siberian Branch of the Russian Academy of Sciences, Russia
[h] Institute for Natural Sciences, North-Eastern Federal University, Yakutsk, Russia
[i] Georesources and Environment Toulouse, GET, UMR5563 CNRS, University of Toulouse, France
[j] N. Laverov Federal Center for Integrated Arctic Research, Arkhangelsk, Russia

Received 26 July 2016; accepted in revised form 7 July 2017; available online 14 July 2017

Abstract

Rivers are significant contributors of Fe to the ocean. However, the characteristics of chemically reactive Fe remain poorly constrained, especially in large Arctic rivers, which drain landscapes highly susceptible to climate change and carbon cycle alteration. The aim of this study was a detailed characterisation (size, mineralogy, and speciation) of riverine Fe-bearing particles (>0.22 μm) and colloids (1 kDa–0.22 μm) and their association with organic carbon (OC), in the Lena River and tributaries, which drain a catchment almost entirely underlain by permafrost. Samples from the main channel and tributaries representing watersheds that span a wide range in topography and lithology were taken after the spring flood in June 2013 and summer baseflow in July 2012. Fe-bearing particles were identified, using Transmission Electron Microscopy, as large (200 nm–1 μm) aggregates of smaller (20–30 nm) spherical colloids of chemically-reactive ferrihydrite. In contrast, there were also large (500 nm–1 μm) aggregates of clay (illite) particles and smaller (100–200 nm) iron oxide particles (dominantly hematite) that contain poorly reactive Fe. TEM imaging and Scanning Transmission X-ray microscopy (STXM) indicated that the ferrihydrite is present as discrete particles within networks of amorphous particulate organic carbon (POC) and attached to the surface of primary produced organic matter and clay particles. Together, these larger particles act as the main carriers of nanoscale ferrihydrite in the Lena River basin. The chemically reactive ferrihydrite accounts for on average 70 ± 15% of the total suspended Fe in the Lena River and tributaries. These observations place important constraints on Fe and OC cycling in the Lena River catchment area and Fe-bearing particle transport to the Arctic Ocean.

Keywords: iron particles; Arctic reactivity; Transmission Electron Microscopy; X-ray Absorption Spectroscopy

* Corresponding author at: Department of Geological Sciences, Swedish Museum of Natural History, 104 05 Stockholm, Sweden.
E-mail address: catherine.hirst@nrm.se (C. Hirst).

http://dx.doi.org/10.1016/j.gca.2017.07.012
0016-7037/

1. INTRODUCTION

Iron enters the ocean via rivers, aeolian dust, ice-rafted sediments, glacial meltwaters and hydrothermal vents at the sea floor (Raiswell and Canfield, 2012). The riverine supply of particulate Fe to the oceans is three orders of magnitude greater than the dissolved Fe (Martin and Meybeck, 1979). These particles span a range in size, mineralogy and speciation (Poulton and Raiswell, 2005), features which together determine their chemical reactivity (Tagliabue et al., 2017). Throughout the environment, reactive Fe-bearing particles, comprised of amorphous to poorly crystalline Fe oxides (e.g. ferrihydrite), represent a potential source of dissolved, bioavailable Fe in soils (Lindsay and Schwab, 1982), rivers (Poulton and Raiswell, 2005) and oceans (Lam and Bishop, 2008) and have mineral surfaces which sequester and transport organic matter (OM) (Lalonde et al., 2012), and trace elements (TE) (Dahlqvist et al., 2007). Upon entering the ocean, Fe-bearing particles sediment onto the continental shelf (Sholkovitz, 1976) and can contribute to a flux of bioavailable Fe released from shelf sediments (Severmann et al., 2006, 2010) or trap labile organic carbon (OC) (Mayer, 1994) which remains metastable in shelf sediments (Lalonde et al., 2012). Thus river-derived Fe-bearing particles contribute to the sequestration of organic carbon into shelf sediments and also play a role in atmospheric carbon dioxide removal (Field, 1998). Understanding the chemical reactivity of Fe-bearing particles in large Arctic river catchments, and so their capacity to sequester or produce OC on the continental shelf of the Arctic Ocean is important for constraining Arctic basin chemical cycles.

Arctic rivers drain a landscape that is highly sensitive to climatic change (Collins et al., 2013). The enhanced surface temperatures across the Arctic (Romanovsky et al., 2010) have resulted in increased river water temperatures (Liu et al., 2005) and increased discharge (Peterson et al., 2002; Yang et al., 2002). There is also an increase in seasonal active layer thickness (Zhang, 2005), in regions that store a substantial amount of OC (Tamocai et al., 2009). Previous studies of Fe-bearing particles and colloids focussed on small Arctic and sub-Arctic rivers and used a variety of size separation techniques to characterise the relationship between Fe and OC (Ingri et al., 2000, 2006; Pokrovsky and Schott, 2002; Pokrovsky et al., 2006, 2010; Vasyukova et al., 2010, 2012; Bagard et al., 2011; Schroth et al., 2011; Ilina et al., 2013; Stolpe et al., 2013; Kritzberg et al., 2014; Escoube et al., 2015). These studies investigated the chemical form of Fe in the dissolved fraction, operationally defined as <0.22 μm or <0.45 μm, which appears to be inorganic Fe oxides or Fe-OC complexes (Ingri et al., 2000, 2006). This is in agreement with laboratory studies showing that Fe is associated with OC during transport in the river system (Hassellöv and von der Kammer, 2008), either as Fe (oxyhydr)oxides or co-precipitated Fe-OC complexes (Gu et al., 1995). Stable Fe-isotope analysis of Fe in the nanoscale particle fractions has also identified low molecular weight (LMW) Fe-OC complexes in Arctic rivers and streams (Ilina et al., 2013). In addition, TEM (Transmission Electron Microscopy) and XAS (X-ray Absorption Spectroscopy) techniques have been used to investigate the relationship between Fe and OC (Rose et al., 1998; Perret et al., 2000), with focus on sub-boreal peatland soils, soil pore water, groundwater, low order streams and lakes (Karlsson et al., 2008; Van Schaik et al., 2008; Karlsson and Persson, 2010; Karlsson and Persson, 2012; Baken et al., 2013; Sjöstedt et al., 2013; Sundman et al., 2014; Herndon et al., 2017). These studies demonstrate that Fe-OC complexation and oxidation state of Fe (Fe(II)/Fe(III)) is governed by the concentration and composition of OC and the pH of the system. However there has been no previous nanoscale analysis of Fe-bearing particles in large Arctic rivers such as the Lena River.

In this study the size, mineralogy, speciation of Fe-bearing particles and their association with OC, are determined in particles from the Lena River main channel and major tributaries draining contrasting mountain and low lying weathering regimes and during the post-spring flood period at the onset of active layer formation and enhanced water-rock interaction. This provides information on chemical reactivity of Fe-bearing particles in Arctic rivers, which is a key to understanding biologically mediated processes occurring in these vast catchment areas and constraining the transport of reactive Fe to the Arctic Ocean.

2. SAMPLE AREA

The Lena River is 4260 km long and has a catchment area of 2.5 million km^2 (Rachold et al., 1996) with an annual discharge to the Arctic Ocean of 581 km^3 (Yang et al., 2002). The catchment is subject to long cold winters (temperatures of −45 °C to −50 °C from November to March) and short hot summers (temperatures of +30 °C to +35 °C from June to August) (Fedorov et al., 2014). The average annual precipitation in the Lena River catchment is 330 mm, with 70–80% occurring during the summer (Chevychelov and Bosikov, 2010). The catchment is almost entirely underlain by permafrost, which extends to depths of up to 1500 m (Anisimov and Reneva, 2006). The permafrost is mainly composed of cryogenic mineral soils: podzols and leptisols in the southern mountains, cambisols in the centre of the basin and gleysols in the northern tundra (Stolbovoi and McCallum, 2002). The active layer varies between 1.4–2.5 m for sandy/clayey soils and 0.6–0.8 m for peat bog soils and thermokarst lakes and bogs are prevalent, especially in the low lying Central Plateau (Huh and Edmond, 1999). Yedoma (Pleistocene windblown deposits) exists along the banks of the Viliui River and in central low lying regions adjacent to the main channel (Grosse et al., 2013). The catchment is dominated by larch and salix forest in the south with exposed rock outcrop in alpine areas and tundra in the north with vegetation of mainly small shrubs, mosses and lichen (Chevychelov and Bosikov, 2010). This study subdivides the data according to the regional geology (Sharoglazov, 1965, 1967) as reported in Table 1.

Table 1
Outline of the studied regions in the Lena River basin, including the number of samples collected, the regional geology and permafrost conditions.

	Number of Samples	Geology and Permafrost
Geographical Region		
Lena River	22	Source in the Trans Baikal Highlands. Talik (unfrozen ground) along the base of the river. Areas of thermal erosion along the banks of the river. Islands formed from Quaternary sand deposits are evident in central section of the main channel (in the region between Yakutsk and the Viliui River tributary)
Aldan River	7	Source in the Verkhoyansk Mountains and Stanovoy-Aldan Shield. Talik (unfrozen ground) along the base of the river. Areas of thermal erosion along the banks of the river. Tributary draining the Verkhoyansk Mountains and Stanovoy-Aldan Shield
Viliui River	5	Source in the Olenëk-Viliui volcanic tableland. Talik (unfrozen ground) along the base of the river. Areas of thermal erosion along the banks of the river. River bank with unconsolidated Quaternary sands
Low lying tributaries		
Central Siberian Plateau	19	Mesozoic terrigenous and carbonate sediments with overlying Quaternary alluvial sediments Evaporite and carbonate karst rocks dominate the south and east of the plateau Continuous permafrost in the north. Intra and supra permafrost groundwater influx in areas of carbonate karst and quaternary sands in the south and east of the plateau. Yedoma permafrost in the Central Yakutian Lowlands, between Yakusk and the Viliui confluence
Mountain tributaries		
Verkhoyansk Mountains	22	Carboniferous and Permian terrigenous sediments Continuous permafrost. Bed rock exposure at high elevations
Stanovoy-Aldan Mountains	1	Proterozoic crystalline and metamorphic rocks (schist, gneiss, quartzite and marble) Discontinuous permafrost. Bed rock exposure at high elevations
Trans Baikal Mountain Range	0	Proterozoic crystalline and metamorphic rocks (schist, gneiss, quartzite and marble) Discontinuous and isolated permafrost. Bed rock exposure at high elevations

3. SAMPLING AND PROCESSING

3.1. Field sampling and measurements

Samples were collected from the Lena River catchment in the post-spring flood period of July 2012 and June 2013 (Fig. 1). The Lena River discharge pattern for 2012 and 2013 is shown in the Electronic Annex (E.A. Fig. 1). River water was sampled at 77 locations and the sampling route is outlined in Fig. 1a and sample locations are shown in Fig. 1b. Sample positions, tributary names, and measured field parameters are reported in E.A. Table 1. All sampling equipment was acid washed using 0.5 M HNO_3 and deionized water. The pH of the water was measured *in-situ* using an YSI® 556 multi probe system (MPS) calibrated with NIST buffer solutions with an accuracy of ±0.03 pH units, along with temperature (accuracy: 0.1 °C) and conductivity (accuracy: 1 µS/cm). Sample positions were taken using a GPS receiver (Garmin® 62), with an accuracy of 50 m.

3.2. Filtration and dialysis

The Fe and OC in river water are subdivided into the following operationally defined fractions:

P[Fe]: particulate Fe (Fe > 0.22 µm)
D[Fe]: dissolved Fe (Fe < 0.22 µm)
HMW D[Fe]: high molecular weight colloidal Fe (0.22 µm–10 kDa)
LMW D[Fe]: low molecular weight colloidal Fe (10 kDa–1 kDa)
TD [Fe]: truly dissolved Fe (<1 kDa)
POC: particulate organic carbon (>0.7 µm)
DOC: dissolved organic carbon (<0.7 µm)
HMW [OC]: high molecular weight colloidal OC (0.7 µm–10 kDa)
LMW [OC]: low molecular weight colloidal OC (10 kDa–1 kDa)
TD [OC]: truly dissolved OC (<1 kDa)

The operationally defined size fractions were separated by filtration and dialysis. The collected waters were filtered on-site within 3 h of sampling through pre-cleaned 142 mm diameter, 0.22 µm nitrocellulose membrane filters (Millipore®). The filters were frozen (−18 °C) immediately after filtration. Water samples were refrigerated (+8 °C) and acidified to pH 2 with ultrapure 8 M HNO_3 (Seastar®) acid three weeks after sampling. After membrane filtration, the dissolved fractions (<0.22 µm) of 29 samples were separated according to the molecular weight of the particles following the method of Pokrovsky et al. (2011) and Vasyukova et al. (2012) using tubular dialysis membranes (Spectrapore 7®), with molecular weight cut-off sizes of 1 kDa and 10 kDa). Prior to use, the membranes were rinsed in 2% HNO_3 and MilliQ® water. The clean membranes were filled with 50 ml of 18 MΩ MilliQ® water, sealed and stored at 8 °C in MilliQ® water filled containers. During sample processing, a MilliQ® water filled membrane was transferred to a 1 L wide mouth bottle containing the <0.22 µm filtered

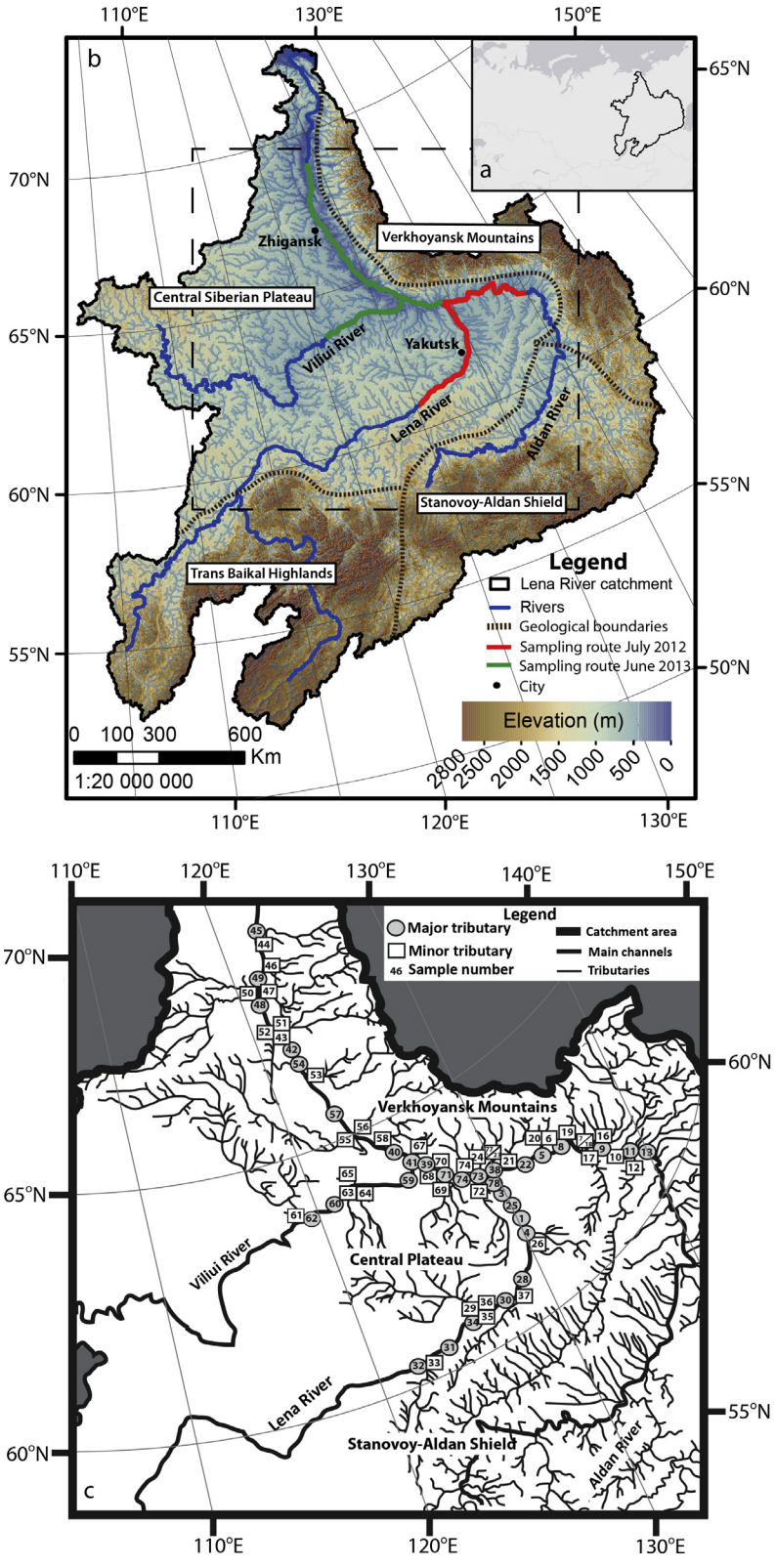

Fig. 1. (a) The Lena River basin with the main channel (Lena River) and major tributaries, (Viliui and Aldan Rivers) marked. Sampling routes from July 2012 and June 2013 are shown. Sampled tributaries are categorised according to their geological units and grouped according to Table 1. (b) Sample stations for main channel and major tributaries (Aldan River and Viliui River) (circles) and minor tributaries (square) draining the Central Plateau, and Stanovoy-Aldan Shield and Verkhoyansk Mountains are shown. Sample numbers correspond to those in Electronic Annex, Table 1.

water sample (with a dilution factor <1.05) and left for 72 h to equilibrate. All handling of membranes and water in the field was carried out in a portable glove box to minimize contamination. The integrity of the dialysis method was tested by comparing the concentrations of major anions (e.g. SO_4^{2-} and F^-) in the dialysis water and in the external solution. The concentrations of SO_4^{2-} and F^- agree within 10%, suggesting that there are minimal membrane charging effects that could affect the distribution of Fe between HMW D[Fe], LMW D[Fe] and TD[Fe]. The combined filtration and dialysis membrane blank for Fe was 2.8 μg/L ($n = 5$), which is only 2% of the average of 0.22 μm filtered Lena River [Fe]. The combined filtration and dialysis membrane blank for OC was 0.4 mg/L ($n = 3$), which is 4% of the average of Lena River [OC]. Samples for DOC were collected using 25 mm, 0.7 μm, pre-combusted glass fiber filters (GF/F) (Whatman®). The filtered waters collected for DOC measurements in 2012 were preserved with phosphoric acid and refrigerated until analysis, while those collected in 2013 were frozen water immediately after collection, alongside the GF/F filters for POC analysis.

The major element analyses (Mg, Ca, Si, Na, K, Al) were done on an ICP-OES (Thermo® ICAP 6500 Duo) with detection limits of 1 ppb and precision of ±5%, estimated from measurements of NIST 1640a. Trace element analyses (Fe, Mn) were performed using an Element 2 sector-field ICP-MS (Thermo®). The detection limit was 0.1 ppb for Fe and Mn. A good agreement was obtained between replicated measurements of SLRS-5 and certified values for ICP-OES and ICP-MS analysis (relative difference <5%, $n = 3$). The DOC was determined by high-temperature catalytic oxidation (Shimadzu® TOC-VCPH) with a detection limit of 0.1 mg/L and an uncertainty of 0.1 mg/L to 2.0 mg/L. The dialysis membrane OC blanks were <0.5 mg/L. The POC concentrations were calculated from the mass of water pumped through the filters and the mass of carbon at the GF/F filters, determined by mass spectrometry (Thermo Finnigan® Delta V Advantage).

3.3. TEM imaging and analyses

Transmission Electron Microscopy (TEM) was used to characterise the particles collected on the >0.22 μm nitrocellulose filters (7 samples) and those in the <0.22 μm water (3 samples). Approximately 3 areas of each filter/water sample were analysed and the images included here are representative of 102 TEM images of particles taken on filters and 28 images of particles in non-acidified filtered waters. Aging effects of Fe oxides after collection were expected to be small since the half-life of transformation to crystalline forms is >500 days when refrigerated or frozen (Hawkings et al., 2014). A 10 mm^2 sample of freeze-dried filter was suspended in 1 ml of MilliQ® water and sonicated to produce a suspension. One drop of the suspension was pipetted onto a carbon film-Cu grid (Agar scientific™) supported on filter paper, and allowed to dry. The Fe-bearing phases in <0.22 μm filtered water were observed on both functionalised positively and negatively charged carbon grids (Dune Sciences). The grids were stirred in the filtered water sample for ~3 min and air-dried prior to TEM. Samples that did not undergo STXM analysis were imaged and analysed using an FEI Tecnai F20 200 kV FEGTEM fitted with a Gatan Orius SC600 CCD camera and an Oxford Instruments X-Max 80 mm^2 Energy Dispersive X-ray (EDX) SDD. Selected Area Electron Diffraction (SAED) patterns were acquired for the particulate material.

3.4. STXM imaging and analysis

TEM and Scanning Transmission X-ray Spectroscopy (STXM) were applied to the same Fe-bearing particles to identify the speciation and coordination of Fe and the association with OC. TEM offers a superior spatial resolution for the imaging of particles but the X-ray specific interaction with particles (via Near Edge X-ray Absorption Fine Structure (NEXAFS) spectroscopy) is superior for determination of the local atomic structure and oxidation state of Fe. Hence, these techniques are complimentary for the analysis of heterogeneous Fe-bearing river particles. The particles were deposited on carbon-coated grids and characterised using a Philips CM20 200 kV TEM. During TEM analysis, care was taken to minimise electron beam damage by optimising the time taken to image and analyse the particles. The same grids were then used to characterise the particles using STXM on beamline I08 at the Diamond Light Source, UK. The I08-STXM is optimised for spectro-microscopy in the 280–4400 eV photon energy range and a spectral resolution of 4000 over the entire photon energy range. Fe L-edge NEXAFS maps with a spatial resolution of 50 nm were collected to study Fe oxidation state and speciation. Stacks of up to 100 STXM energies were acquired at different photon energies, and the NEXAFS spectra was depicted from the image stack for each pixel of the raster scan using computational program, Mantis (Lerotic et al., 2014). XRF elemental mapping was also used to determine the association of carbon, oxygen, nitrogen and iron within the areas studied. Caution must be taken when interpreting particle associations following filtration, freezing and TEM analysis. However, sampling and imaging procedures used here are consistent with those used in previous studies (Allard et al., 2004; Toner et al., 2009; Von der Heyden et al., 2012, 2014) where little alteration of the sample during sampling and analysis was reported.

3.5. Chemical separation of particulate material

Particulate material from 36 sample stations was dissolved in order to quantify the Particulate [Fe] fraction. The total particle dissolution procedure is described in E.A. Fig. 2. The sample handling was conducted in Class 100 laminar flow hoods, and ultrapure acids (Seastar®) and water (18 MΩ MilliQ®) were used throughout preparations and analysis. Typically, two filters were analysed from each station. One filter underwent total dissolution, using HCl, HNO_3 and HF to determine the P[Fe]. The total filter dissolution method was tested using three standards (E.A. Table 2). Recoveries of Fe for the dissolution of BCR-1 (Columbian River Basalt) and W2 (Diabase) were 97% ($n = 8$) and 90% ($n = 7$), respectively. The average acid

blank for filter dissolution was 0.3 μg Fe/filter ($n = 10$), and blank for a 0.22 μm nitrocellulose filter, washed in 5% acetic acid, was 1.8 μg Fe/filter ($n = 7$). The acid and filter blank correction was on average 0.6% of the P[Fe].

Thereafter, Particulate [Fe] was chemically separated to quantify the reactive, poorly crystalline Leach P[Fe] from the poorly reactive, crystalline Residual P[Fe] (E.A. Fig. 2). A second filter, from the same sample location, was leached using 0.5 M HCl at room temperature for 24 h (Leventhal and Taylor, 1990; Lam and Bishop, 2008). This method was used previously for the separation of amorphous and poorly crystalline Fe in isotope studies (Rouxel et al., 2005; Severmann et al., 2006; Wiederhold et al., 2007; Fehr et al., 2008, 2010). To test the reliability of this Fe separation, aluminium which is mainly incorporated in the silicate fraction of riverine particles (Taylor and McLennan, 1985), was analysed in the leach and residual fractions of 27 samples. The Residual P[Fe] fractions had <70% of Al (E.A. Fig. 3). The remaining Al has been removed during leaching and either corresponds with Al that substitutes for Fe in the structure of poorly crystalline Fe (oxy)hydroxides or the leaching of the clay particle fraction (Schwertmann et al., 1979). Hence, the chemical separation represents the upper limit of chemically reactive Fe on the filters. The mass balance: Total P[Fe] = Leach P [Fe] + Residual P[Fe] was assessed for 13 filters. The average difference between Total P[Fe] and (Leach P[Fe] + Residual P[Fe]) was 25% (±10%).

4. RESULTS

Iron is mainly found in the Particulate [Fe] and HMW Dissolved [Fe] fractions (Fig. 2, Table 2). The proportion of Fe in the different size fractions is the same irrespective of region in the catchment (Fig. 2), with on average 70% of the Total [Fe] hosted in the particulate fraction ($n = 36$, $2\sigma = 17\%$). For samples that underwent dialysis, the HMW D[Fe] constitutes 90% ($n = 26$, $2\sigma = 10\%$) of the dissolved Fe and only 4% ($n = 26$, $2\sigma = 4\%$) of this D [Fe] is found as truly dissolved TD[Fe]. The mineralogy, morphology and speciation of Fe-bearing particles and their association with OC, were determined in the particulate material and non-acidified filtered waters in mountain tributaries (LR51, LR44, LR70, LR17), low lying tributaries (LR52, LR43, LR62) and the main Lena River channel (LR75, LR45). There were no observed differences in the mineralogy, morphology and speciation of Fe-bearing particles between samples collected in June 2013 and July 2012.

4.1. Mineralogy and morphology of Fe-bearing particles

TEM imaging allows the identification of amorphous and poorly crystalline particles. Fig. 3 shows examples of poorly crystalline chemically reactive Fe-bearing particle aggregates which span a range in size from ~1 μm to 20 nm. The particles are aggregates of individual nanoparticles, <10 nm in size (Fig. 3a) and the Selected Area Electron Diffraction (SAED) pattern for these nanoparticles (Fig. 3b) shows two broad rings at 0.18 nm and 0.28 nm. The EDX spectrum (Fig. 3c) shows peaks at Fe and O from iron (oxyhydr)oxide. Mg, P, S, Ca, Al, Si, and K are commonly associated with the larger (>0.22 μm) particles and likely reflect a trace element signature from associated clay minerals. The larger aggregates of ferrihydrite span a range of aggregate shapes (Fig. 4a–c), including 100–200 nm long angular aggregates of ferrihydrite (Fig. 4a), highly spherical aggregates of ferrihydrite (Fig. 4b) and poorly defined aggregate shapes (Fig. 4c), all of which are common in all samples. In contrast, the smaller 20–30 nm particles, composed of Fe and O, are consistently sub-rounded to rounded in shape (Fig. 4d–f). In combination, these observations demonstrate the presence of 2-line ferrihydrite mineralogy (Janney et al., 2000; Hawkings et al., 2014) in the P

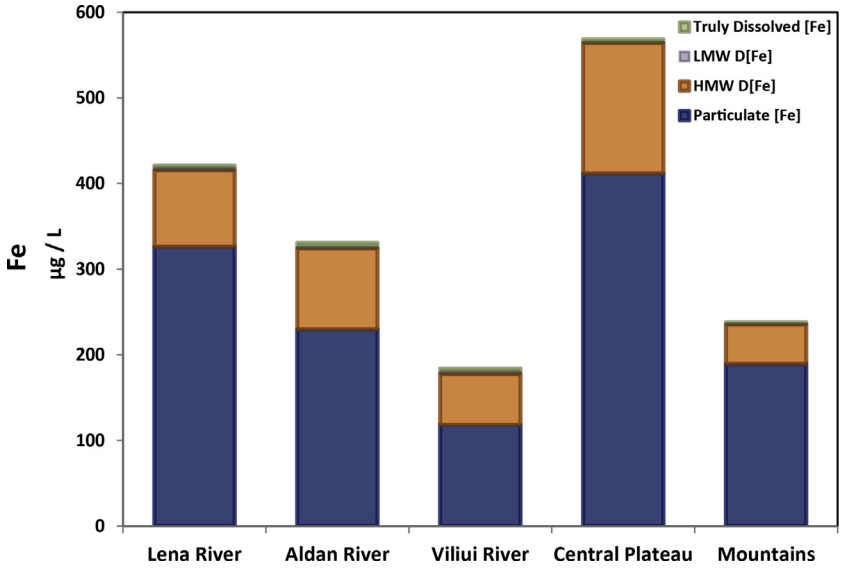

Fig. 2. Bar chart showing the average concentration of Fe in different size fractions: Particulate [Fe] (>0.22 μm), HMW D[Fe] (<0.22 μm–10 kDa), LMW D[Fe] (<10 kDa–1 kDa), TD[Fe] (<1 kDa). Note < 1 kDa ~ 1.3 nm size. All data is reported in the E.A. Table 3.

Table 2
Fe concentrations in the particulate (P[Fe]), leached (Leach P[Fe]), residual (Residual P[Fe]) and dissolved (D[Fe]) fraction for the 36 samples, for which particulate analysis was done. The proportion of residual and leached Fe is given as a percentage (%) of the particulate Fe, P[Fe]. and the proportion of particulate and dissolved iron is given as a percentage (%) of the total iron, Total [Fe]. Samples that were not analysed are denoted with ***. All percentages (%) are stated to the nearest 10%, to reflect the uncertainty in chemical extraction of reactive Fe, inherent to the cold HCl leach.

	[Fe]				Fraction of Particulate [Fe]		Fraction of Total [Fe]		Fraction of Total [Fe]	
Lena River	Particulate µg/L	Residual	Leach	Dissolved	Total	Residual %	Leach %	Dissolved %	Particulate %	Reactive %	Non Reactive %
LR78	160	70	84	34	190	40	50	20	80	60	40
LR31	340	170	160	88	420	50	50	20	80	60	40
LR42	32	15	10	130	150	50	30	80	22	90	10
LR57	330	190	140	65	400	60	40	20	90	50	50
LR45	270	130	140	84	350	50	50	20	80	60	40
LR4	520	390	200	160	750	80	40	20	90	50	50
LR2	470	460	200	100	760	100	40	20	80	40	***
LR1	450	270	180	110	560	60	40	20	80	50	50
LR71	80	***	***	70	***	***	***	50	50	***	***
Average	300	210	140	90	450	60	40	30	70	60	40
Standard Deviation (2σ)	170	150	70	40	230	20	7	20	20	20	14
Aldan River											
LR5	220	100	60	110	270	50	30	30	70	60	40
LR8	360	120	70	110	300	30	20	20	80	60	40
LR13	120	***	40	80	120	200	30	40	60	***	***
Average	230	110	57	100	230	93	30	30	70	60	40
Standard Deviation (2σ)	120	10	15	10	100	93	6	10	10	0	0
Viliui River											
LR59	360	80	80	30	190	20	20	10	90	60	40
LR60	80	***	***	80	80	***	***	***	***	***	***
Average	220	80	80	50	140	20	20	30	90	60	40
Standard Deviation (2σ)	200	***	***	60	80	***	***	30	30	***	***
Central Plateau											
LR55	390	80	350	200	630	20	90	30	70	90	10
LR63	220	30	230	190	450	10	90	50	50	90	10
LR50	190	80	100	130	310	40	50	40	60	70	30
LR52	270	60	200	170	430	20	70	40	60	90	10
LR69	70	20	50	50	120	30	70	50	60	80	20
LR65	480	90	490	290	870	0	100	40	60	90	10
LR72	150	***	***	80	150	***	***	40	70	***	***
LR61	1200	***	***	80	1200	***	***	8	90	***	***
LR37	1600	900	480	110	1600	60	***	7	***	***	***
LR26	180	***	***	110	180	***	***	40	60	***	***
LR43	200	***	***	170	370	***	***	50	50	***	***

Average	240	60	240	140	570	30	70	40	70	90	15	
Standard Deviation (2σ)	130	29	160	70	470	20	30	10	20	10	8	
Verkhoyansk Mountains												
LR58	220	120	100	70	290	60	50	20	80	60	40	
LR56	200	80	120	20	220	40	60	10	90	60	40	
LR67	170	60	110	40	210	40	70	19	90	70	30	
LR16	460	120	160	90	370	30	40	20	80	70	30	
LR53	360	160	200	20	380	40	60	5	100	60	40	
LR46	170	80	150	80	310	50	90	30	70	70	30	
Average	260	100	140	50	300	40	60	20	90	70	35	
Standard Deviation (2σ)	120	40	40	30	70	10	20	10	10	10	5	
Stanovoy-Aldan Shield												
LR33	30	15	10	21	46	50	30	46	60	70	30	
LR12	30	11	12	21	45	40	40	40	60	70	30	
LR27	70	27	22	61	110	40	30	50	50	70	30	
Average	43	18	15	34	70	40	30	50	60	70	30	
Standard Deviation (2σ)	23	8	6	23	40	5	5	5	5	0	0	

[Fe] and HMW D[Fe] size fractions, in all analysed filters and filtered water.

Crystalline Fe oxide particles are rarely observed but hematite was identified in the particulate material from two samples in tributaries draining the Verkhoyansk Mountains (LR44, LR51) (Fig. 5a). These 80–100 nm rounded particles were identified by the distinct SAED pattern with major diffraction rings at 0.75 nm, 0.45 nm, 0.40 nm, 0.35 nm, 0.31 nm (Fig. 5b). Goethite was observed in particulate material from a tributary draining the Central Plateau (LR62) (Fig. 5d), identified by the more crystalline SAED pattern (Fig. 5g) and needle-like arrangement of nanoparticles (Fig. 5e and f). The goethite in Fig. 5d is adjacent to the surface of a microbe. These crystalline Fe oxides are less chemically reactive than the poorly crystalline ferrihydrite. Elements associated with the hematite particles include Mg, Al, Si, P, S, Ca, Ti and Mn and the goethite particles, Al, Si, P, Ca (Fig. 5c and h).

Two chemically distinct types of clay particles were identified in the Lena River and major tributaries. Fig. 6a shows an aggregate of clay particles from the Verkhoyansk Mountains (LR51) composed of Al, Si, O and also Fe, Ca and K (Fig. 6b). The composition and particle morphology are consistent with the mineral illite. In contrast, an aggregate of 400 nm wide clay particles, from the Central Plateau (LR62) (Fig. 6d) has a hexagonal SAED pattern and subeuhedral hexagonal shape (Fig. 6e). These clay particles contain Al, Si and O, with no additional cations detected via EDX, (Fig. 6f). The composition and morphology of these particles is indicative of the mineral kaolinite. These two distinct types of clay particles, illite and kaolinite, were observed in all analysed tributaries and the main channel. Aggregates of 20–100 nm ferrihydrite are associated with the surface of both clay particles (Fig. 6c and g).

4.2. Speciation of Fe in poorly crystalline particles

The poorly crystalline Fe-bearing particles (Fig. 3a) were analysed via STXM to determine the oxidation state of Fe. A 0.5 μm particle from the Lena River main channel (LR70) is shown in Fig. 7a. The XRF map (Fig. 7b) confirms that the particle contains Fe and O. Spectra from Fe-bearing particles in the Verkhoyansk Mountains and Lena River particulate material (>0.22 μm) are shown in Fig. 7c alongside the spectra for Fe-bearing particles from the south Atlantic and Southern Ocean (Von der Heyden et al., 2012). This comparison suggests that the Fe-bearing particles in these Arctic rivers contain only Fe(III), as is expected within the structure of ferrihydrite (Jambor and Dutrizac, 1998) and thus consistent with the TEM characterisation.

4.3. Relationship between Fe-bearing particles and organic carbon

The size distribution of OC in the Lena River and major tributaries is shown in Fig. 8. POC constitutes 7% of the TOC while 70% of the TOC is in the LMW [OC] and TD [OC] fractions (<10 kDa), with 60% in the smallest, <1 kDa size fraction. Hence, Fe and OC are observed in

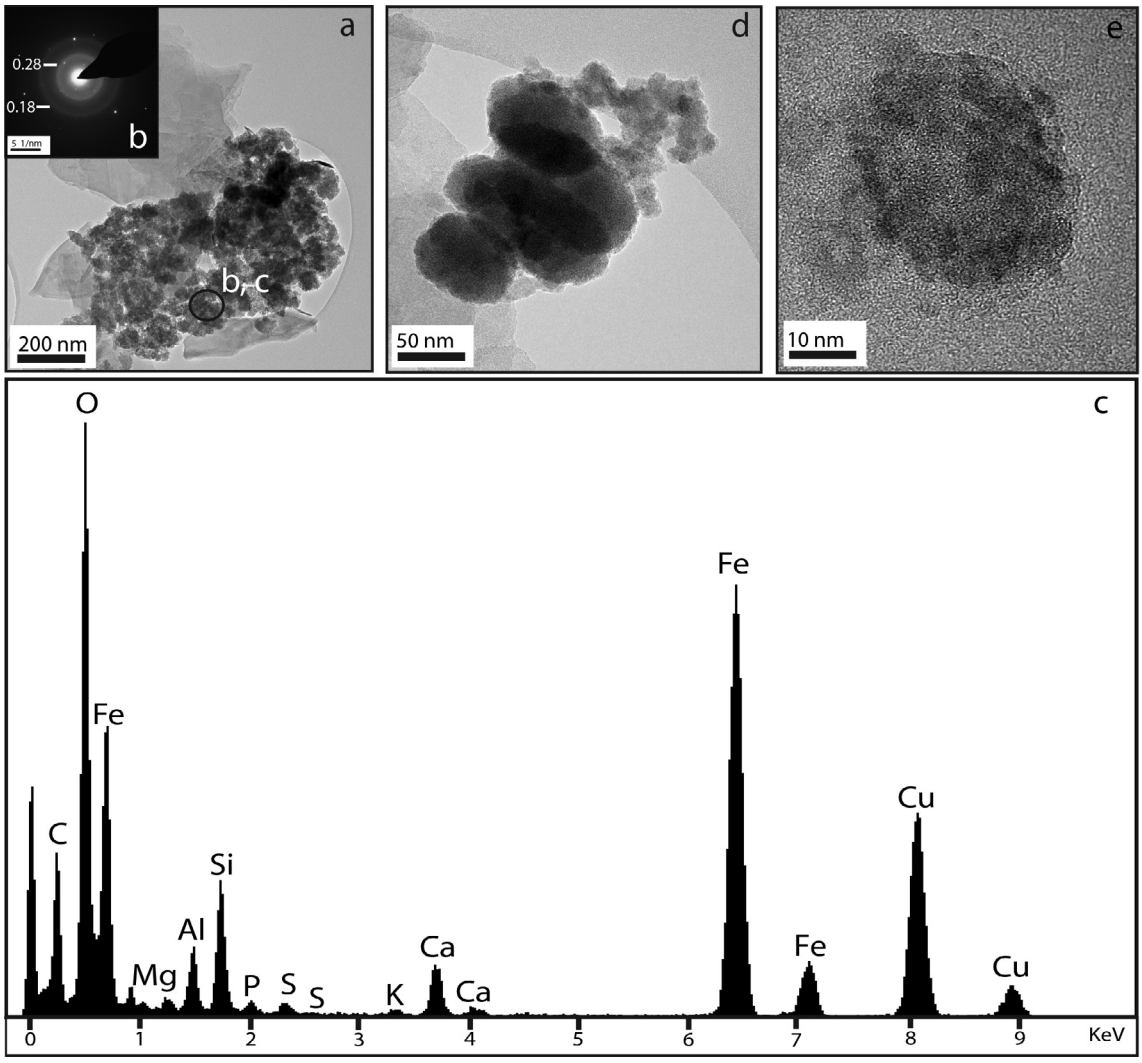

Fig. 3. TEM images showing chemically reactive Fe-bearing particles which range in size from 1 μm to 20 nm collected on a 0.22 μm nitrocellulose filter (a–d) and in <0.22 μm non-acidified filtered water (e). All particles are composed of aggregates of smaller nanoparticles. There is no evidence of crystal lattice fringes on the nanoparticles and the diffraction pattern (b) only shows rings at 0.18 nm and 0.28 nm, which demonstrate that the particles are amorphous to poorly crystalline. The EDX spectra (c) shows peaks corresponding to Fe and O and minor peaks in C, Mg, Al, Si, P, S, K, Ca. The combined information is indicative of a 2-line ferrihydrite, a chemically reactive particle. The Cu signal comes from the underlying copper grid.

different operationally defined size fractions, with Fe predominantly in the particulate fraction and HMW colloidal fraction and OC in the dissolved fraction. Despite the low contribution, POC is similar in size to the identified Fe-bearing particles and therefore a potential surface on which the P[Fe] can bind. Three forms of POC structures were commonly observed on nitrocellulose 0.22 μm filters: (i) diatom frustules, (ii) networks of elongate fibrils, and (iii) microorganisms (Fig. 9). Micron-sized bacterial cells and diatoms were commonly observed in the Central Plateau tributaries, whereas, >5 μm wide, web-like structures of organic fibrils were observed in all particulate material. Notably, clusters of darker particles, approximately 50–150 nm in size, were associated with the OC network (Fig. 10a), and XRF mapping (Fig. 10b) showed that these aggregates are Fe-rich. The Fe L-edge NEXAFS spectra (Fig. 10c) from each identified Fe aggregate (Fig. 10b) were compared with the spectra from south Atlantic and Southern Ocean particles (Von der Heyden et al., 2012) (Fig. 7) and are all consistent with Fe(III) species, with no evidence of mixed valence or Fe(II) species. TEM imaging at higher magnification (Fig. 10d) indicated that these particles are nano-crystalline and similar to the ferrihydrite aggregates observed in the <0.22 μm fractions (Fig. 3e). The combined information in Fig. 10 shows that ~50 nm wide aggregates of ferrihydrite can be dispersed within the network of POC, as well as aggregating to form larger ferrihydrite particles, as seen in Fig. 3a.

4.4. Quantifying the different forms of Fe-bearing particle

The poorly crystalline ferrihydrite (Leach P[Fe]) was chemically separated from crystalline Fe oxides and clays (Residual P[Fe]). In all tributaries and the main channel,

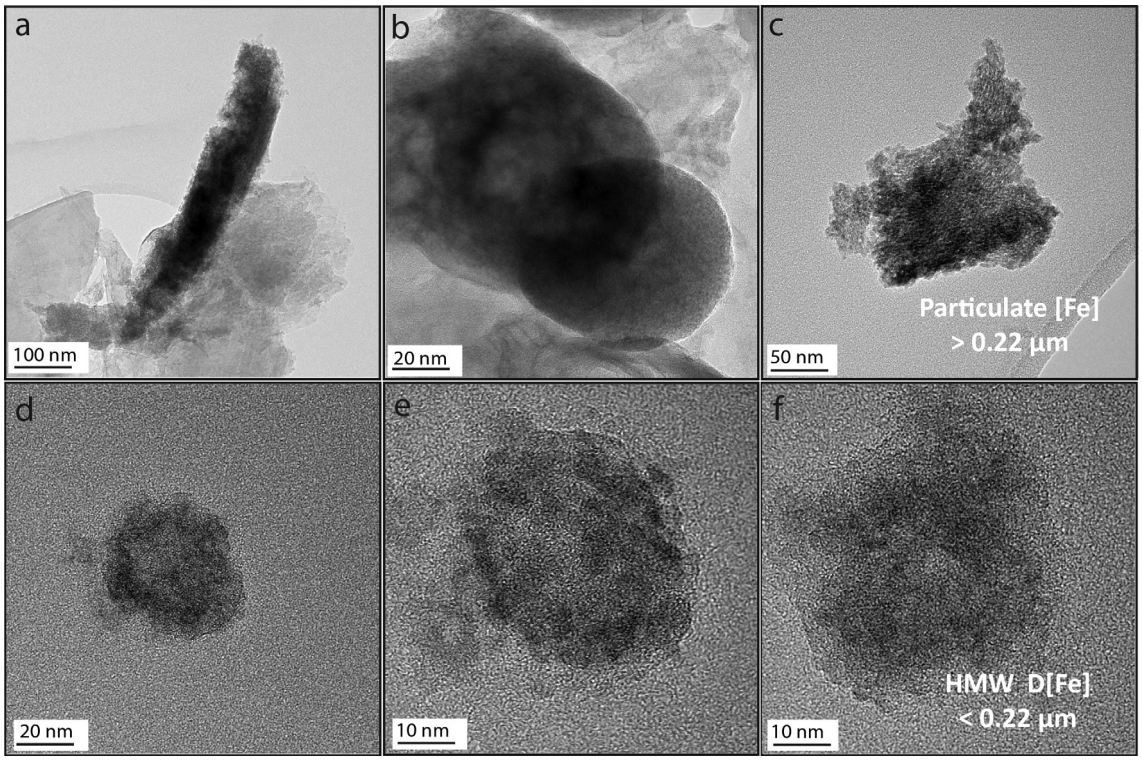

Fig. 4. TEM images (a–c), from 0.22 µm nitrocellulose filters, show 500 nm–100 nm aggregates of ferrihydrite with different morphologies. Image (a) shows an elongated particle associated with a clay mineral phase; Image (b) shows two rounded nanoparticles with highly uniform edges, each is 80–100 nm wide; Image (c) shows an aggregate of ferrihydrite nanoparticles with no clear structure or defined edges, but the appearance of lattice fringes suggests that this particle is more crystalline and corresponds with an aged form of ferrihydrite. TEM images (d–f), from non-acidified, 0.22 µm filtered water, show 30–10 nm aggregates of ferrihydrite with a rounded to sub-rounded morphology. The larger aggregates of ferrihydrite nanoparticles (in P[Fe]) have broader range of particle morphology than the smaller aggregates (in HMW D [Fe]).

there is an equal contribution of Residual P[Fe], (30%, $n = 26$, $2\sigma = 15\%$), Leach P[Fe], (35%, $n = 26$, $2\sigma = 20\%$), and HMW D[Fe], (30% ($n = 26$, $2\sigma = 15\%$) to the Total [Fe] (Fig. 11). The remaining Fe is in the LMW D[Fe] and TD D[Fe] fractions (Fig. 2). On average, the Central Plateau tributaries contribute the highest concentrations of Leach P[Fe], 240 µg/L, $2\sigma = 160$ µg/L, and Dissolved [Fe], 140 µg/L, $2\sigma = 70$ µg/L. Together these fractions have been identified as chemically reactive ferrihydrite (Fig. 3) which spans a size range from 1 µm to 20 nm particles with no observable differences in the mineralogy, morphology and speciation of Fe-bearing particles between regions. This chemically reactive fraction contributes 90% of the Total [Fe] in Central Plateau tributaries, 70% of the Total [Fe] in Verkhoyansk Mountains and Stanovoy-Aldan Shield tributaries, and 60% of the Total [Fe] in the Lena River, Aldan River and Viliui River (Table 2).

5. DISCUSSION

The particulate fraction contains the largest proportion (70% ±20%) of Fe in the Lena River and tributaries. A substantial proportion of the Fe in the particulate (>0.22 µm) and HMW colloidal (0.22 µm–10 kDa) fractions is in a chemically reactive form, primarily ferrihydrite that comprises ≥60% of the Fe-bearing particles transported in the Lena River and major tributaries, during the post-spring flood period (Fig. 11). All ferrihydrite spans a size range from 1 µm to 20 nm particles with no observable differences in the mineralogy, morphology and speciation of Fe-bearing particles between regions. The characteristics of these Fe-bearing particles are compared with previous studies of Fe-bearing particles and organic carbon in other global river systems and also discussed in terms of their importance for the transport of Fe to the continental shelf.

5.1. The chemical reactivity of Fe-bearing particles

The ferrihydrite aggregates show distinct size fractions including 20–30 nm wide particles corresponding to the HMW colloidal Fe fraction; and larger aggregates (100–200 nm and 500 nm–1 µm) that are the main contributor to the leached particulate Fe (Fig. 3a). The size range of ferrihydrite aggregates is consistent with the "fractal organisation of Fe into primary, intermediate and secondary aggregates" observed during synthetic studies of ferrihydrite formation (Guénet et al., 2017). The aggregated nature of smaller particles (Fig. 3d and e) indicates that the surface charge of ferrihydrite is neutralised, which inhibits the repulsive forces between colloids and favours their

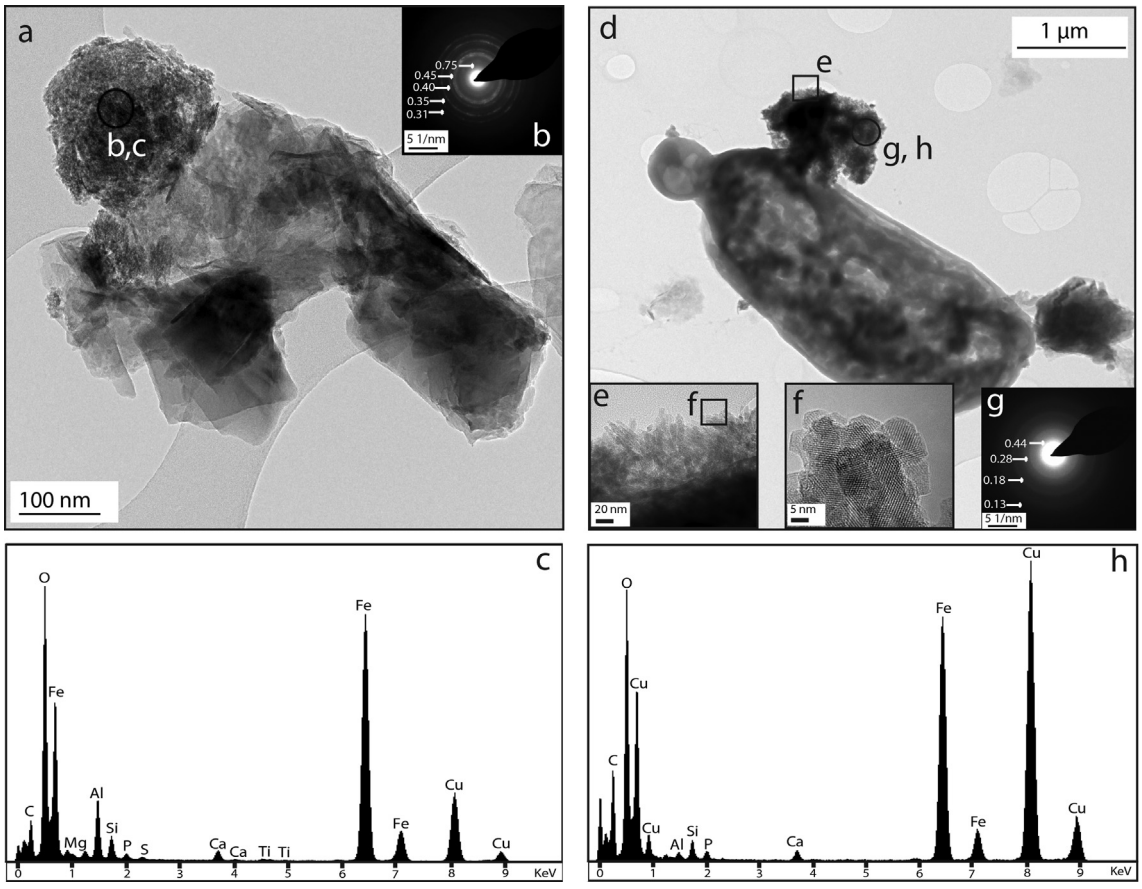

Fig. 5. TEM images showing poorly reactive crystalline Fe-oxide particles collected on 0.22 µm nitrocellulose filters. TEM image (a) shows an aggregate of hematite, only observed in *Verkhoyansk Mountains* tributaries (LR44, LR70, LR51). The particle is a sub-rounded, 100 nm wide Fe oxide aggregate attached to the surface of a clay particle. The iron oxide has a diffraction pattern (b) representative of hematite, with diffraction rings at 0.75 nm, 0.45 nm, 0.40 nm, 0.35 nm, 0.31 nm. The hematite aggregate has associated trace elements Mg, Al, Si, P, S, Ca, Ti and Mn. TEM image (d) shows a dark, poorly crystalline particle attached to the surface of a microbial cell. This is nano-particulate goethite composed of needle-like nano-crystals (e, f) and a diffraction pattern with multiple rings at 0.13 nm, 0.18 nm, 0.28 nm and 0.44 nm (g). The particle is attached to the surface of a microbial cell and was observed in a tributary draining the *Central Plateau* (LR43).

aggregation (Banfield et al., 2000), to form the larger (500 nm–1 µm) aggregates. A low surface charge on colloids is favoured at the near neutral pH of the Lena River waters (E.A. Table 1), which are close to the point of zero (PZC) charge for ferrihydrite, pH ~ 7 to 8 (Stumm and Morgan, 1996). Ferrihydrite is metastable and the chemical reactivity of Fe tends to decrease via aggregation and recrystallization of the poorly ordered ferrihydrite (Banfield et al., 2000) to form the more crystalline and thus less bioavailable Fe oxide particles (e.g. hematite, Soltis et al., 2016), observed in Fig. 5. However, these crystalline forms of Fe oxide were rarely observed in the particulate material, indicating that the residence time of Fe-bearing particles in the Lena river basin is not sufficient to allow recrystallisation into thermodynamically more stable forms. Instead, ferrihydrite is stabilised via attachment to clay particles (Fig. 6) as previously observed in the Amazon River (Allard et al., 2004) and glacially-fed rivers (Poulton and Raiswell, 2005). The clay particles and diatom tests are also a source of silica (Cornell, 1987), phosphorous and sulphur (Borch et al., 2007), which are incorporated in the ferrihydrite structure (Fig. 3c) and can inhibit recrystallisation to less reactive forms (Zhao et al., 1994).

The relationship between organic carbon and Fe-bearing particles will influence the chemical reactivity of the Fe (Perret et al., 2000). Previous studies of lake, soil and river waters show that organic carbon either prevents the polymerization of Fe(oxyhydr)oxides, by forming smaller Fe-OC complexes or provides a "template for formation and growth" of Fe (oxyhydr)oxides (Perret et al., 2000), as is also documented in soils (Chen et al., 2016), deltaic (Shields et al., 2016) and marine sediments (Lalonde et al., 2012). Ferrihydrite in the Lena River and major tributaries is observed as smaller 50 nm particle aggregates embedded in networks of organic carbon (Fig. 10), rather than complexed with Fe-OC in smaller size fractions (Fig. 3a). This is similar to previously observed particles in temperate lakes (Perret et al., 2000) and the tropical Rio Negro (Allard et al., 2004), where ferrihydrite is located within "biopolymer and diffuse organic matter domains". The consistency of ferrihydrite-organic carbon association in tropical and temperate waters as well as Arctic rivers

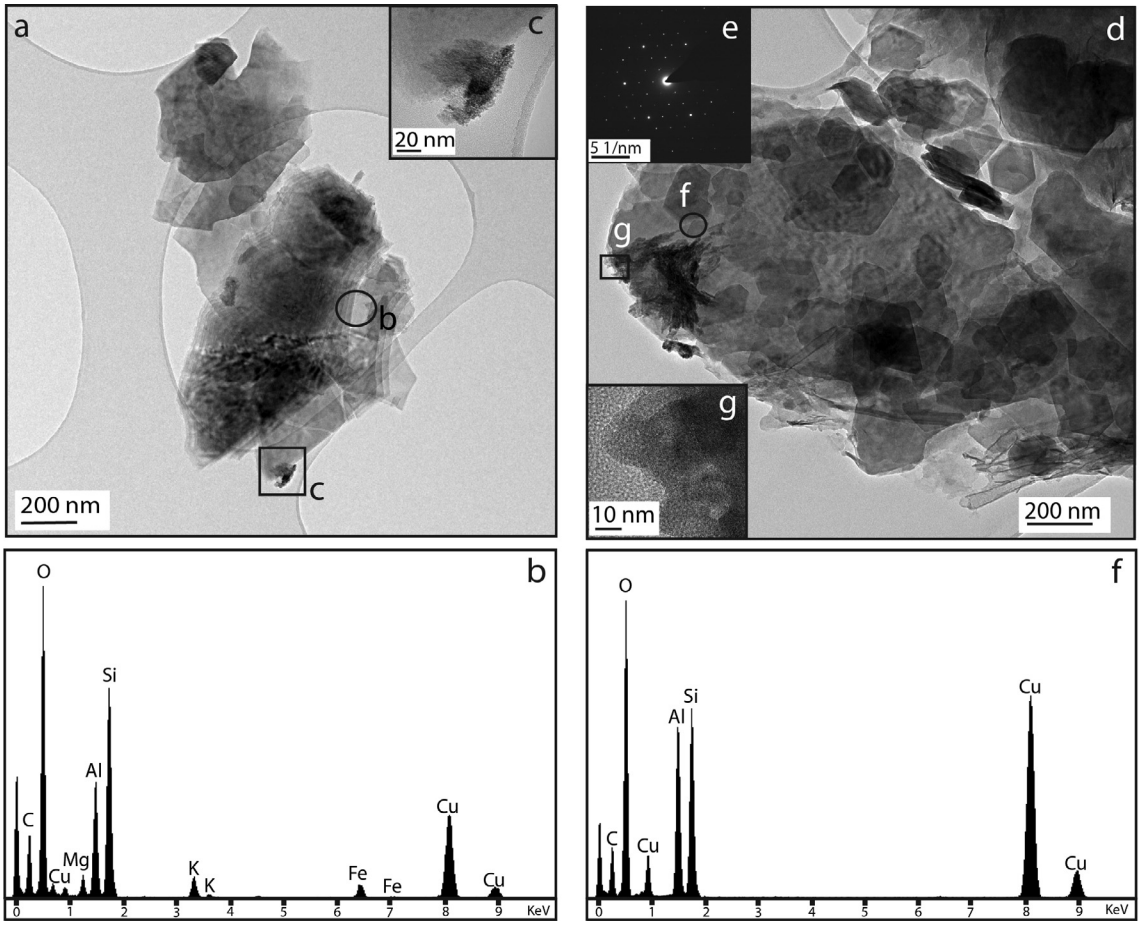

Fig. 6. TEM images of clay particles from 0.22 μm nitrocellulose filters. TEM image (a) shows 300–400 nm sheets of clay particles. The EDX spectra (b) shows that these particles contain Al, Si, O and also K, Ca, Fe and C. Figure (c) shows a 20 μm aggregates of ferrihydrite attached to the surface of this clay particle aggregate. TEM image (d) shows an aggregation of euhedral hexagonal shaped clay particles. Individual particles are typically 100–300 nm wide and aggregate to form particles >1 μm. The hexagonal diffraction pattern (e) shows that this particle is crystalline and EDX spectra (f) shows that it contains Al, O and Si but no interstitial Fe within the crystalline structure. A 100 nm aggregate of ferrihydrite (g) is attached to the surface of the clay particle aggregate. Both examples of clay particles were observed on all analysed filters.

draining permafrost terrain suggests a similar mechanism of Fe(III) mobilisation from soils and transport in organic-rich natural waters. The association tends to reduce the size of ferrihydrite aggregates, preventing lattice reorganisation (Chen et al., 2016), and so maintain higher Fe reactivity. Indeed, experimental studies show that organic fibrils can nucleate ferrihydrite and produce nanometer sized particles (Schwertmann et al., 2005; Guénet et al., 2017). The dispersed nanoparticles of ferrihydrite in Fig. 10 may have formed contemporaneously with the OC fibrils, or attached to the surface of the OC after formation.

Microbial cells (Fig. 9e and f) are observed in all tributaries and the Lena River main channel. Fe-bearing particles are sometimes found associated with the surface of these cells. The nanoparticles are attached to the cell surface (Fig. 5d) rather than embedded inside the cells, indicating ferrihydrite was formed in the soil or water column, and subsequently attached to the surface of the microorganism (Glasauer et al., 2001) rather than forming *in-situ* by biomineralisation as has also been suggested (Fortin and Langley, 2005). The morphology of ferrihydrite particles becomes more irregular with increased aggregation (Fig. 4a–c). This may affect the interaction between Fe and POC during transport, where the smaller, sub rounded aggregates attach to the surface of POC but larger irregularly shaped aggregates of ferrihydrite were not (Figs. 4d–f, and 10d). This autochthonous POC plays a role in the transport of ferrihydrite, especially in the rivers draining the Central Plateau where microbial cells are most commonly observed. Overall, the association between ferrihydrite, POC and clay particles may hinder aggregation that promotes recrystallization and so can help to sustain Fe in a reactive form during transport in the Lena River and major tributaries.

5.2. Comparison with Fe and OC in other systems

The (20 nm–1 μm) aggregates of ferrihydrite observed in this study are similar in size to particles identified in previous nanoscale analyses of reactive Fe, at the outflow of South African rivers, (Von der Heyden et al., 2012), large tropical rivers (Benedetti et al., 2003; Allard et al., 2004),

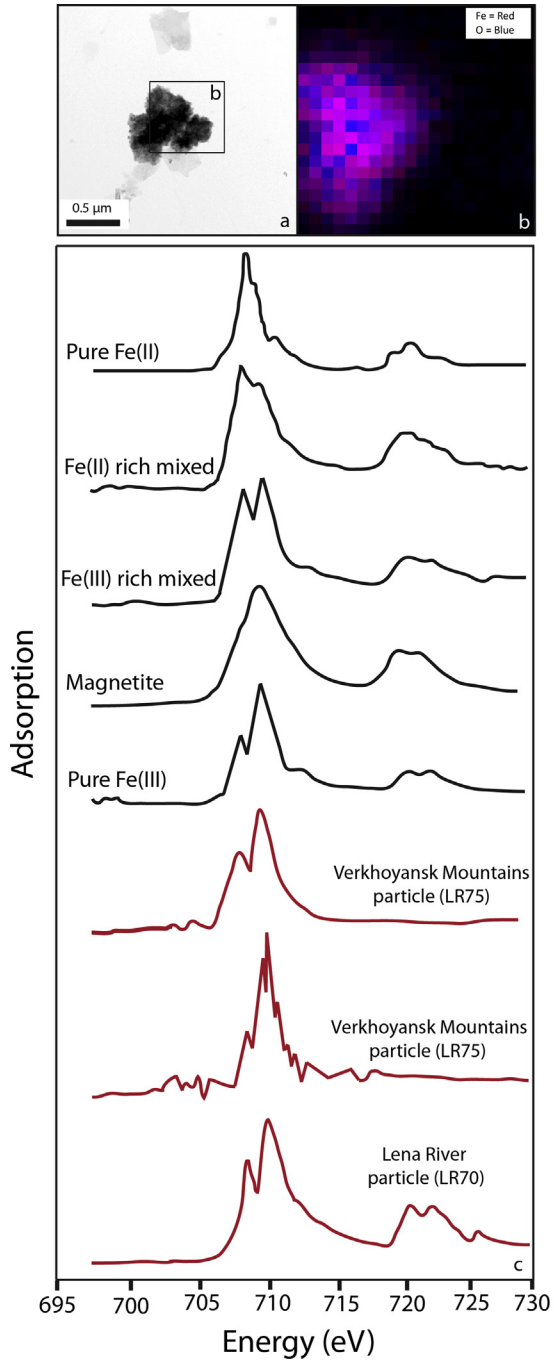

Fig. 7. The speciation of chemically reactive Fe-bearing particles. TEM image (a) shows a Fe-bearing particle from the *Lena River main channel* (LR75). (b) The XRF mapping shows that this particle is composed of Fe and O. (c) The speciation of chemically reactive Fe-bearing particles in the *Lena River main channel* (LR70) and *Verkhoyansk Mountains* (LR75) (in red), was determined using NEXAFS spectra. These are compared with the Fe L-edge XANES spectra of Fe-bearing particles from the south Atlantic and Southern Ocean (Von der Heyden et al., 2012) The NEXAFS spectra in Fe-bearing particles from LR70 and LR75 are indicative of Fe (III) oxides, in the form of poorly crystalline ferrihydrite. (For interpretation of the references to colour in this figure legend, the reader is referred to the web version of this article.)

temperate rivers (Poulton and Raiswell, 2005), glacially-fed rivers (Poulton and Raiswell, 2005; Hawkings et al., 2014; Hodson et al., 2017) and headwater streams of the permafrost-bearing zone of western Siberia (Pokrovsky et al., 2016). These Fe-bearing particles are composed of Fe^{3+} and not complexed with OC, which is in contrast with Fe-bearing particles in aerosols (Schroth et al., 2009; Oakes et al., 2012), hydrothermal plumes (Toner et al., 2009), ocean water (Von der Heyden et al., 2012, 2014), subtropical lakes (Von der Heyden et al., 2014), smaller temperate rivers (Krachler et al., 2016) and boreal rivers (Neubauer et al., 2013) where Fe is mainly in the form of Fe–OC complexes and in a reduced Fe(II) or mixed Fe(II)/Fe(III) state.

The Fe in the Lena River and major tributaries is dominantly in the particulate fraction (Fig. 2), similar to the Severnaya Dvina River, the largest European Arctic river (Pokrovsky et al., 2010), where >60% of Fe is transported in particulate form, as well as to the Amazon River, where >90% of Fe is supplied in particulate form (Allard et al., 2004). The Fe-bearing particles in the Lena River basin show a similar range in size, mineralogy, speciation and association with OC, irrespective of their origin in mountains or low lying regions. The concentration of dissolved Fe in the Lena River basin is similar to that of the other large Arctic rivers sampled during the post-spring flood period (Martin et al., 1993; Guieu et al., 1996; Ingri et al., 2000; Pokrovsky et al., 2006, 2010; Escoube et al., 2015) but the size distribution of dissolved Fe is offset from the size distribution of DOC in all of these large river systems, where Fe is mainly found in the large-size colloids (10 kDa–0.22 µm) and DOC is primarily carried in the truly dissolved, <1 kDa size. The TEM and STXM analyses demonstrate that the smallest observed ferrihydrite aggregates, 20 nm–30 nm colloidal particles, are not associated with OC (Fig. 5) and Fe is present in an oxidised (Fe(III)) form (Fig. 8), consistent with indirect observations of 4–40 nm wide inorganic Fe-bearing particles in the Yukon River (Stolpe et al., 2013), in larger permafrost-free boreal rivers (Vasyukova et al., 2010), and in permafrost-dominated boreal rivers of the Central Siberian Plateau (Pokrovsky et al., 2006). These observations are in contrast to those of soils, soil pore waters and first order streams in temperate, sub-boreal and boreal regions of Northern Sweden and western Russia, where up to 60% of the colloidal fraction is in the form of smaller Fe-OC complexes with Fe in both Fe(II) and Fe(III) oxidation states (Karlsson and Persson, 2010; Ilina et al., 2013; Neubauer et al., 2013; Sundman et al., 2014). This suggests alteration of Fe-bearing particles occurs during transport from headwaters to the Lena River.

In general, the concentration of OC is higher in first order streams than large Arctic rivers (Denfeld et al., 2013; Mann et al., 2015) that have a greater connectivity with the OC-rich riparian and hyporheic zones (Creed et al., 2015) and have low D[Fe]/DOC ratios (Neubauer et al., 2013). Fe(II)- OC co-precipitation is more common (Gu et al., 1995) in soil porewaters in these zones because high DOC concentrations maintain a low oxygen environment in the soil. The suboxic or anoxic groundwater provides a source of dissolved Fe which complexes with high molecular weight OC in the soils (Neubauer et al., 2013).

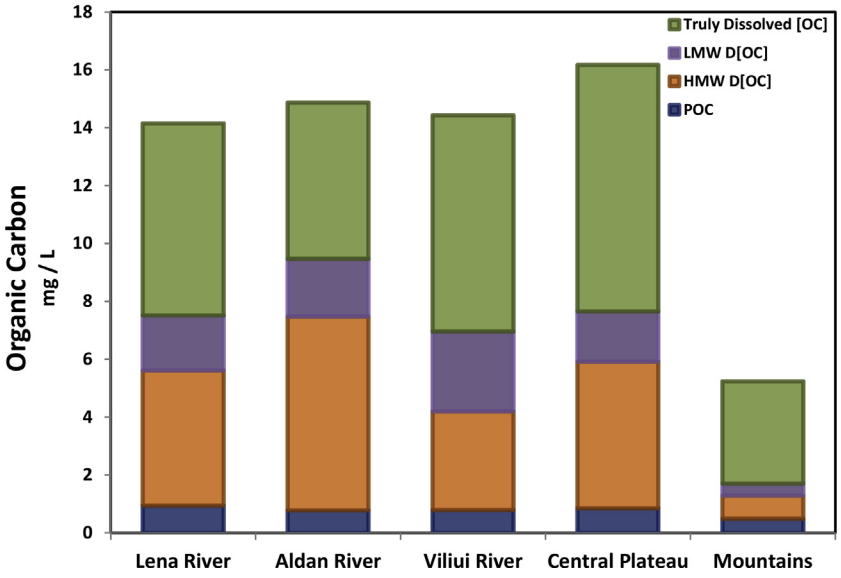

Fig. 8. Bar chart showing the average concentration of organic carbon (OC) in different size fractions, POC (>0.7 μm), HMW DOC (<0.7 μm–10 kDa), LMW DOC (10 kDa–1 kDa), TD DOC (<1 kDa). Note <1 kDa ~ 1.3 nm size (Guo and Santchi, 2007). All data is reported in E.A. Table 3.

The Fe-OC compelxes are sustained in these soil pore waters because the high DOC concentrations maintain a low oxygen environment in the soil (Sundman et al., 2014), resulting in stream waters with low D[Fe]/DOC ratios (Neubauer et al., 2013). The large proportion of OC in the truly dissolved fraction of Lena River waters (Fig. 8) may result from microbial or photo-degradation of OC in the soil or river (Kopácek et al., 2005), as well as from contributions from groundwaters in deeper, mineral-rich horizons (Striegl et al., 2005; Mann et al., 2012). The Fe in Fe-OC complexes binds to carbohydrate groups in the OC (Gu et al., 1995), which are consumed by microbial processing during transport (Mann et al., 2015; Spencer et al., 2015; Drake et al., 2015), suggesting that there is less available OC to bind with Fe in larger rivers as a result of degradation (Creed et al., 2015). Additionally, the pH values in the Lena River catchment area range from 6.3 to 9.4, which are greater than pH values found in soil pore waters, thermokarst lakes and first order streams in boreal rivers (Pokrovsky et al., 2011; Vasyukova et al., 2012). Compiled data of Fe-OC complexation and pH measurements from tropical, temperate and boreal rivers show that Fe-OC complexation decreases with increasing pH for all rivers due to more pronounced hydrolysis and polymerization of Fe(III) in the form of colloidal oxy(hydr)oxides (Lofts et al., 2008; Neubauer et al., 2013). This is especially visible in <1 kDa organic-rich fraction of various organic-rich boreal waters (Vasyukova et al., 2012). Although Sundman et al. (2014) observe that >50% of the Fe is in the form of Fe-OC complexes at pH 6.8 in a low order, sub-boreal stream, these streams have a high concentration of humic-rich OC that favours Fe(III)-OC complexation.

Fe-bearing particles can also originate from areas with less favourable conditions for nanoscale Fe-OC complexation. These include the mechanical weathering of thin mineral-rich soils in the mountainous regions (Huh et al., 1998), mechanical weathering of the main channel river bank and islands (Costard et al., 2003), and the discharge of partially anoxic supra-permafrost and talik-derived groundwaters (Bagard et al., 2011). Goethite forms by the dissolution and recrystallisation of ferrihydrite particles, catalyzed by adsorbed Fe(II) (Schwertmann and Murad, 1983; Yee et al., 2006) in anoxic conditions. The time scale of ferrihydrite transformation to goethite is on the order of weeks (Cornell and Schwertmann, 1996) in oxic soils but may be slower in the recently frozen active layer soils with temperatures near 0 °C in spring. This is longer than the predicted transport time of suspended particles through the Lena River, as it takes 12 ± 4 days for particles to travel 2000 km along the river main channel (Sharoglazov, 1965, 1967). Therefore, the rare observation of aged ferrihydrite and goethite indicate that these Fe-bearing particles formed and aged in the active layer soil profile prior to being washed out into the river system. Hematite is only observed in particulate material of the tributaries from the eastern Verkhoyansk Mountain Range. The formation of hematite requires a rearrangement of the ferrihydrite poorly ordered crystal lattice (Schwertmann and Murad, 1983), and is commonly a product of weathering of Fe-rich sedimentary rocks. Hematite, alongside the clay particles, contributes to the poorly reactive fraction of Fe-bearing particles.

The origin and transport of OC may change due to the effects of future warming in the region, with predictions suggesting (i) enhanced thermal and mechanical erosion of river banks and islands which may contribute a source of labile OC, especially in yedoma regions (Costard et al., 2007; Vonk et al., 2013) and (ii) enhanced degradation of OC in low order streams (Frey et al., 2016), which may reduce the contribution of labile OC to high order streams. Evidence presented here suggests that both responses to cli-

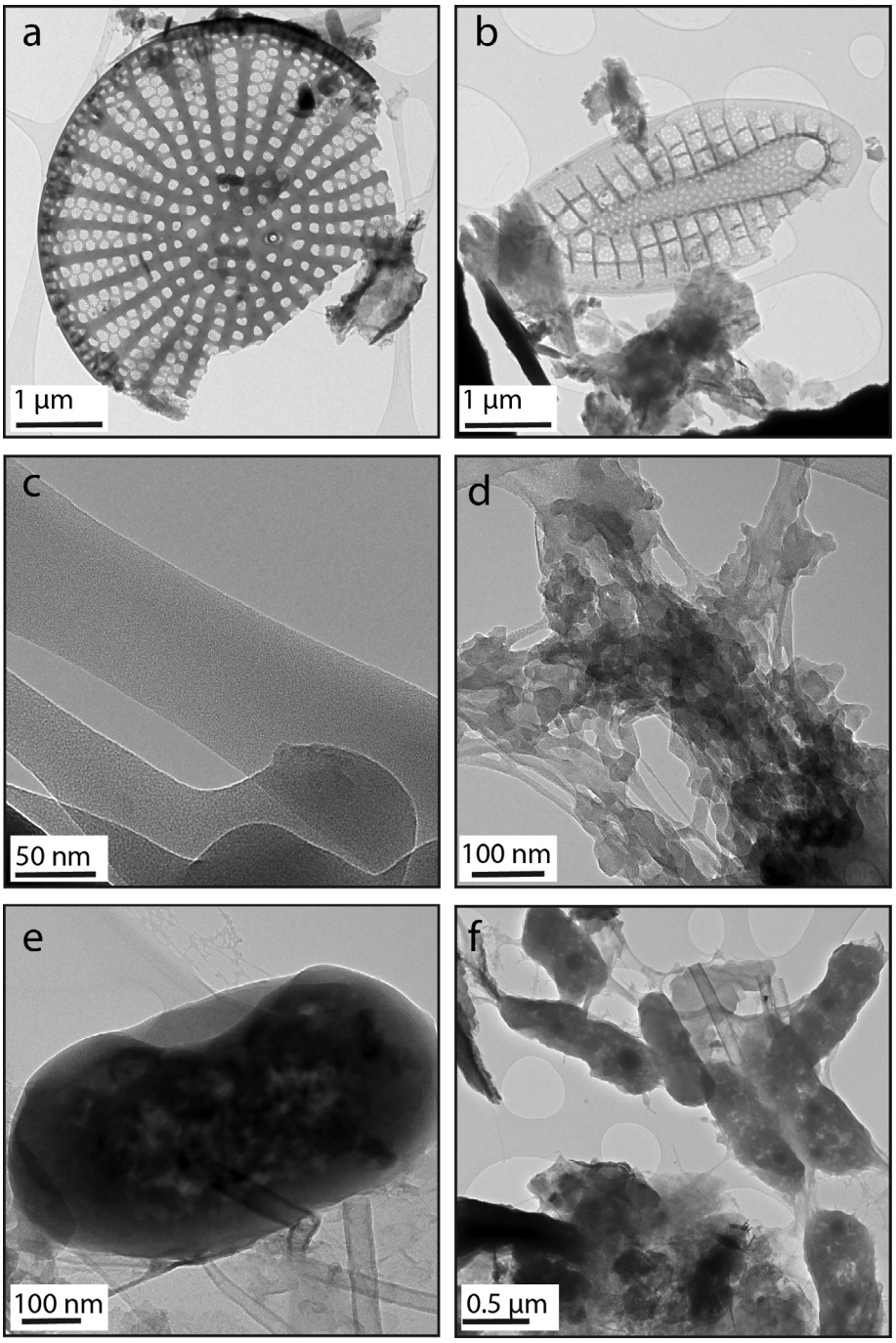

Fig. 9. TEM images of organic matter (OM) on 0.22 µm nitrocellulose filters. The organic matter has a similar size to the largest aggregates of Fe-bearing particles identified in Figs. 3–5. TEM images (a and b) show diatom tests that were observed in all observed tributaries. TEM images (c and d) show networks of organic fibrils which was commonly observed in particulate material from the *Verkhoyansk Mountain* tributaries. TEM images (e and f) show microbial cells, most commonly observed in *Central Plateau* tributaries.

matic change may alter the size, structure and speciation of Fe-bearing particles and the form of OC to which they associate.

5.3. Transport of Fe-bearing particles to the Arctic Ocean

The Fe-bearing particles are transported from the Lena River to the Laptev Sea in the Arctic Ocean. In the estuarine mixing zone, flocculation of colloidal Fe results in a loss of up to 80% of the Fe during transport from the Lena River delta towards regions of high salinity (Martin et al., 1993). Low molecular weight (<1 kDa) Fe-OC complexes behave more conservatively (Pokrovsky et al., 2014) across the salinity gradient compared to high molecular weight colloids and larger Fe-bearing particles. However, in this study less than 5% of Fe is associated with OC in the truly

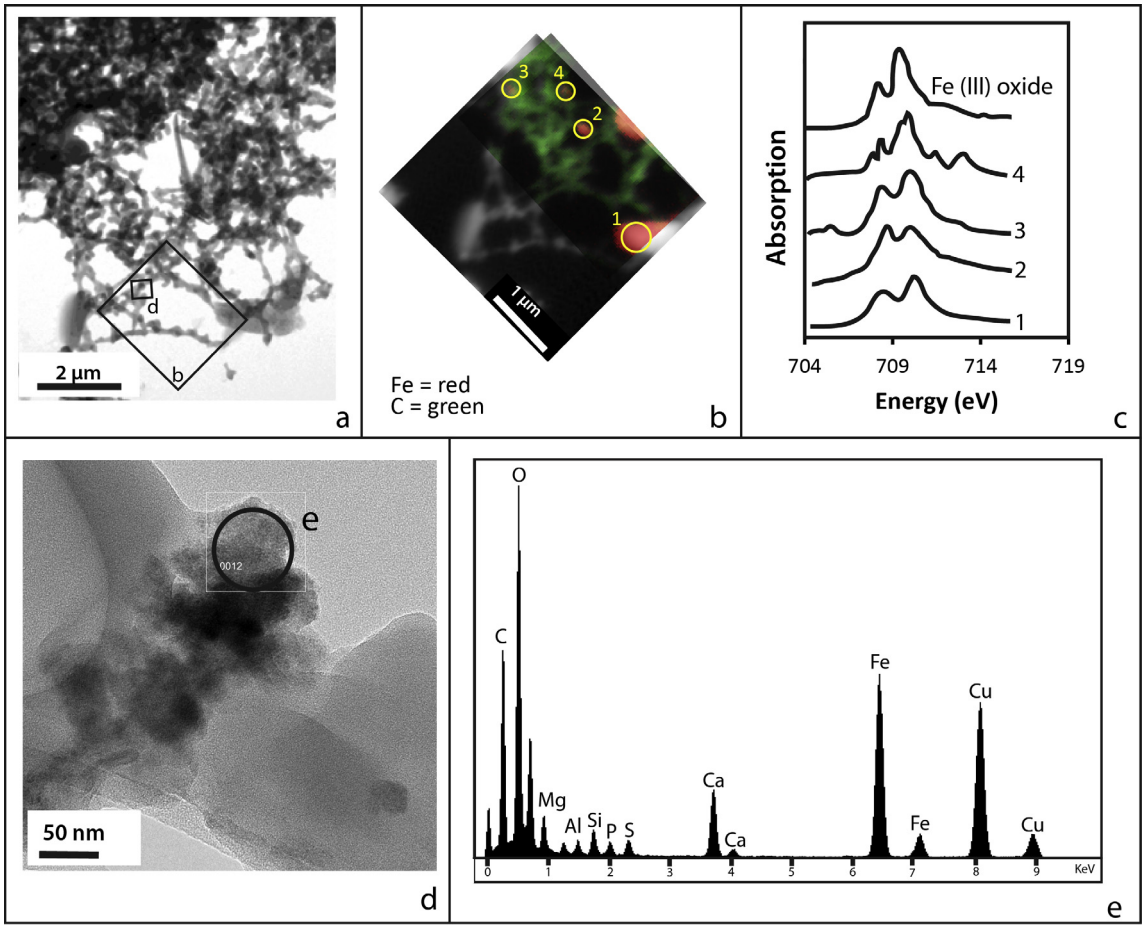

Fig. 10. TEM image (a), from a 0.22 µm nitrocellulose filter, shows a web-like particle from the *Verkhoyansk Mountain* tributary (LR70). Darker "inclusions" were observed within the particle and analysed with STXM. (b) Combined STXM and XRF map shows a carbon-rich region (highlighted in green). Iron-rich regions are dispersed amongst the carbon, (in red). The NEXAFS spectra in (c) correspond to STXM map in (b). These spectra were taken on the Fe L-edge. The spectra (c) indicate that these Fe-rich inclusions are Fe (III) rich particles, which is consistent with the evidence for ferrihydrite. Figure (d) shows a TEM image of these poorly crystalline ferrihydrite particles attached to the OC surface and the EDX spectra (e) shows the presence of C, O, Cu, Mg, Al, Si, P, S, Ca and Fe. The organic fibril is trapping discrete nanoparticulate ferrihydrite particles and there is no evidence of Fe-OC complexation or a reduced or mixed valence Fe (Fe(III) and Fe(II)). (For interpretation of the references to colour in this figure legend, the reader is referred to the web version of this article.)

dissolved (LMW) fraction and instead Fe is associated with micron-sized fibrous organic networks, less susceptible to particle collision and flocculation (Perret et al., 2000). POC is transported from the Lena River to the Laptev Sea (Sánchez-García et al., 2011; Bröder et al., 2016) and about 13% of soil derived POC from the Lena River is associated with "ultrafine" <3.8 µm, reactive Fe-bearing particles in the Laptev Sea (Tesi et al., 2016). This study demonstrates that reactive Fe-bearing particles, spanning a range of aggregate size and shape, are associated with both POC and clay particles. The attachment of POC to flocculating ferrihydrite aggregates reduces the density of the iron (oxyhydr)oxide flocs, allowing them to be transported across the continental shelf (Passow, 2004). Moreover, clay particles, which dominate the speciation of Fe-bearing particles in the Lena River main channel, may also be transported via attachment to POC and thus contribute to the preservation of OC on the continental shelf by providing a surface that reduces exposure of OC to degradation in shelf sediments (Lalonde et al., 2012). The aggregated nanoscale Fe-bearing particles, associated with clays and organics, can be transported beyond the estuarine mixing zone over the continental shelf (Guieu et al., 1996), or contribute to the resuspension or formation of Fe-bearing particles in the continental shelf sediments (Salvadó et al., 2015). This study demonstrates that during the post-spring flood period of 2012 and 2013, on average 70% of particulate Fe in the Lena River main channel is in a reactive form. This form contributes significantly to the bioavailable particulate Fe in the Lena River estuary and may be transported further into the Laptev Sea via either resuspension from sediments or being associated with POC and clay particles.

6. CONCLUSIONS

A range of particle size and chemical separation techniques and nanoscale analysis (TEM and STXM) on an

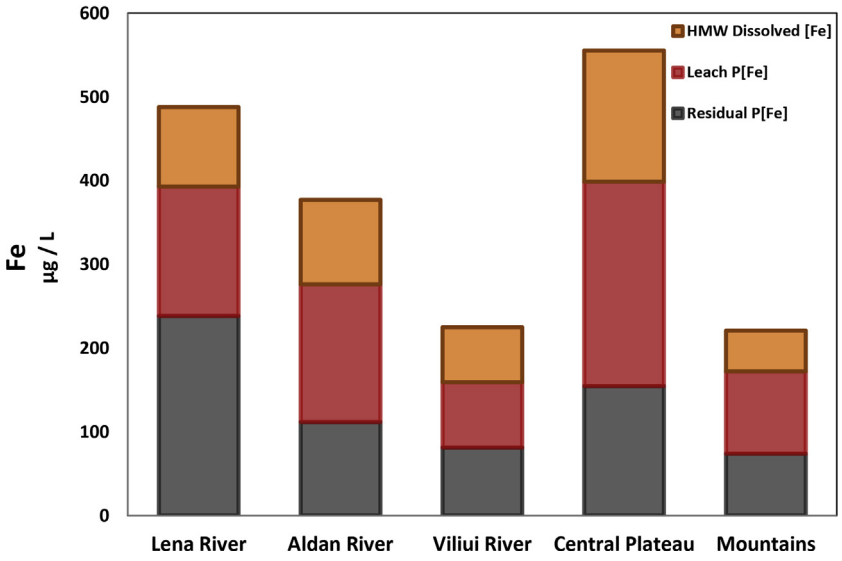

Fig. 11. Bar chart showing the average concentration of Fe in the HMW Dissolved (<0.22 µm), Leach P[Fe] (0.5 M HCl, room temperature, 24 h), and the Residual P[Fe] (HNO_3, HCl, HF dissolution). The size separation protocol and chemical separation method is outlined in E.A. Fig. 2. All data, including standard deviations, is outlined in Table 2.

extensive sample set provides a detailed characterisation of the Fe-bearing particles in the Lena River Basin. The results demonstrate that reactive Fe is ubiquitously in the form of ferrihydrite particles, with a size range of 20 nm to 1 µm, in the main channel and major tributaries. Ferrihydrite constitutes the dominating Fe contribution (70 ± 15%) to the total Fe in tributaries draining varying latitude and topography. These results differ from studies of Fe particles in low order streams, lakes and soil pore waters in sub-boreal systems, where Fe is predominantly found to be complexing with OC. Ferrihydrite persists and does not recrystallize in high order waterways, such as the Lena River and its tributaries due to the favourable conditions derived from the association of ferrihydrite with the surface of POC and clay minerals. The association between 50 and 100 nm ferrihydrite aggregates and networks of organic fibrils observed in the POC suggests that the reactive Fe is predominantly transported via surface attachment to POC rather than LMW DOC complexes with DOC. The present paper presents a synoptic study of Fe across the Lena River basin, providing the first data on the characteristics of Fe across this remote region. Further work is required to confirm that the Fe characteristics observed are the same throughout the year, especially during the spring flood, where a substantial portion of Fe is discharged from the watershed. These findings show that the size and mineralogy of Fe-bearing particles are important for element transport in the Lena River and provide a link between low order boreal rivers and the Arctic Ocean.

ACKNOWLEDGEMENTS

This study was funded by MetTrans, (a European Union Seventh Framework Marie Curie ITN) [Grant No. 290336] and the Swedish Research Council [VR 621-2010-3917]. Beamtime was funded by the Diamond Light Source [Grant No. SP11282]. We thank Burkhard Kaulich, Majid Abyaneh and Tohru Araki on beamline I08 at the Diamond Light Source, Hardwell Science and Innovation campus, for instrument operation and data processing, and Bart van Dongen for initiating the synchrotron work and participation in a beamtime session. A special thanks to the crew of R/V "Merzlotoved", Karin Wallner, Hans Schöberg, Phil Holdship and Mike Ward for their technical support.

APPENDIX A. SUPPLEMENTARY MATERIAL

Supplementary data associated with this article can be found, in the online version, at http://dx.doi.org/10.1016/j.gca.2017.07.012.

REFERENCES

Allard T., Menguy N., Salomon J., Calligaro T., Weber T., Calas G. and Benedetti M. F. (2004) Revealing forms of iron in river-borne material from major tropical rivers of the Amazon Basin (Brazil). *Geochim. Cosmochim. Acta* **68**, 3079–3094.

Anisimov O. and Reneva S. (2006) Permafrost and changing climate: the Russian perspective. *AMBIO: J. Hum. Environ.* **35**, 169–175.

Bagard M. L., Chabaux F., Pokrovsky O. S., Viers J., Prokushkin A. S., Stille P., Rihs S., Schmitt A. D. and Dupré B. (2011) Seasonal variability of element fluxes in two Central Siberian rivers draining high latitude permafrost dominated areas. *Geochim. Cosmochim. Acta* **75**, 3335–3357.

Baken S., Sjöstedt C., Gustafsson J. P., Seuntjens P., Desmet N., De Schutter J. and Smolders E. (2013) Characterisation of hydrous ferric oxides derived from iron-rich groundwaters and their contribution to the suspended sediment of streams. *Appl. Geochem.* **39**, 59–68.

Banfield J. F., Welch S. A., Zhang H., Ebert T. T. and Penn R. L. (2000) Aggregation-based crystal growth and microstructure development in natural iron oxyhydroxide biomineralization products. *Science* **289**, 751–754.

Benedetti M. F., Ranville J. F., Allard T., Bednar A. J. and Menguy N. (2003) The iron status in colloidal matter from the Rio Negro, Brasil. *Colloids Surfaces A Physicochem. Eng. Asp.* **217**, 1–9.

Borch T., Masue Y., Kukkadapu R. K. and Fendorf S. (2007) Phosphate imposed limitations on biological reduction and alteration of ferrihydrite. *Environ. Sci. Technol.* **41**, 166–172.

Bröder L., Tesi T., Salvadó J. A., Semiletov I. P., Dudarev O. V. and Gustafsson O. (2016) Fate of terrigenous organic matter across the Laptev Sea from the mouth of the Lena River to the deep sea of the Arctic interior. *Biogeosciences* **13**, 5003–5019.

Chen K.-Y., Chen T.-Y., Chan Y.-T., Cheng C.-Y., Tzou Y.-M., Liu Y.-T. and Teah H.-Y. (2016) Stabilization of natural organic matter by short-range-order Fe hydroxides. *Environ. Sci. Technol.* **50**, 12612–12620.

Chevychelov A. P. and Bosikov N. P. (2010) Natural conditions. In *The Far North*. Springer, Netherlands, pp. 1–23.

Collins M., Knutti R., Arblaster J., Dufresne J.-L., Fichefet T., Friedlingstein P., Gao X., Gutowski W. J., Johns T., Krinner G., Shongwe M., Tebaldi C., Weaver A. J. and Wehner M. (2013) Long-term climate change: projections, commitments and irreversibility. In *Clim. Chang. 2013 Phys. Sci. Basis. Contrib. Work. Gr. I to Fifth Assess. Rep. Intergov. Panel Clim. Chang.*, pp. 1029–1136.

Cornell R. M. (1987) Effect of silicate species on the transformation of ferrihydrite into goethite and hematite in alkaline media. *Clays Clay Miner.* **35**, 21–28.

Cornell R. M. and Schwertmann U. (1996) *The Iron Oxide*. VCH, New York, p. 377.

Costard F., Dupeyrat L., Gautier E. and Carey-Gailhardis E. (2003) Fluvial thermal erosion investigations along a rapidly eroding river bank: application to the Lena River (Central Siberia). *Earth Surf. Process. Landforms* **28**, 1349–1359.

Costard F., Gautier E., Brunstein D., Hammadi J., Fedorov A., Yang D. and Dupeyrat L. (2007) Impact of the global warming on the fluvial thermal erosion over the Lena River in Central Siberia. *Geophys. Res. Lett.* **34**, 2–5.

Creed I. F., McKnight D. M., Pellerin B. A., Green M. B., Bergamaschi B. A., Aiken G. R., Burns D. A., Findlay S. E., Shanley J. B., Striegl R. G. and Aulenbach B. T. (2015) The river as a chemostat: fresh perspectives on dissolved organic matter flowing down the river continuum. *Can. J. Fish. Aquat. Sci.* **72**, 1272–1285.

Dahlqvist R., Andersson K., Ingri J., Larsson T., Stolpe B. and Turner D. (2007) Temporal variations of colloidal carrier phases and associated trace elements in a boreal river. *Geochim. Cosmochim. Acta* **71**, 5339–5354.

Denfeld B. A., Frey K. E., Sobczak W. V., Mann P. J. and Holmes R. M. (2013) Summer CO_2 evasion from streams and rivers in the Kolyma River basin, north-east Siberia. *Polar Res.* **32**.

Drake T. W., Wickland K. P., Spencer R. G., McKnight D. M. and Striegl R. G. (2015) Ancient low–molecular-weight organic acids in permafrost fuel rapid carbon dioxide production upon thaw. *Proc. Natl. Acad. Sci.* **112**, 13946–13951.

Escoube R., Rouxel O. J., Pokrovsky O. S., Schroth A., Max Holmes R. and Donard O. F. X. (2015) Iron isotope systematics in Arctic rivers. *CR Geosci.* **347**, 377–385.

Fedorov A. N., Ivanova R. N., Park H., Hiyama T. and Iijima Y. (2014) Recent air temperature changes in the permafrost landscapes of northeastern Eurasia. *Polar Sci.* **8**, 114–128.

Fehr M. A., Andersson P. S., Hålenius U. and Mörth C. M. (2008) Iron isotope variations in Holocene sediments of the Gotland Deep, Baltic Sea. *Geochim. Cosmochim. Acta* **72**, 807–826.

Fehr M. A., Andersson P. S., Hålenius U., Gustafsson O. and Morth C. M. (2010) Iron enrichments and Fe isotopic compositions of surface sediments from the Gotland Deep, Baltic Sea. *Chem. Geol.* **277**, 310–322.

Field C. B. (1998) Primary production of the biosphere: integrating terrestrial and oceanic components. *Science (80)* **281**, 237–240.

Fortin D. and Langley S. (2005) Formation and occurrence of biogenic iron-rich minerals. *Earth-Sci. Rev.* **72**, 1–19.

Frey K. E., Sobczak W. V., Mann P. J. and Holmes R. M. (2016) Optical properties and bioavailability of dissolved organic matter along a flow-path continuum from soil pore waters to the Kolyma River mainstem, East Siberia. *Biogeosciences* **13**, 2279–2290.

Glasauer S., Langley S. and Beveridge T. J. (2001) Sorption of Fe (Hydr) oxides to the surface of *Shewanella putrefaciens*: cell-bound fine-grained minerals are not always formed De Novo Sorption of Fe (Hydr) oxides to the surface of *Shewanella putrefaciens*. *Appl. Environ. Microbiol.* **67**, 5544–5550.

Grosse G., Robinson J. E., Bryant R., Taylor M. D., Harper W., DeMasi A., Kyker-Snowman E., Veremeeva A., Schirrmeister L. and Harden J. (2013) Distribution of late Pleistocene ice-rich syngenetic permafrost of the Yedoma Suite in east and central Siberia, Russia. *US Geol. Surv. Open File Rep.* **2013**, 1–37.

Gu B., Schmitt J., Chen Z., Liang L. and McCarthy J. F. (1995) Adsorption and desorption of different organic matter fractions on iron oxide. *Geochim. Cosmochim. Acta* **59**, 219–229.

Guénet H., Davranche M., Vantelon D., Gigault J., Prévost S., Taché O., Jaksch S., Pédrot M., Dorcet V., Boutier A. and Jestin J. (2017) Characterization of iron–organic matter nanoaggregate networks through a combination of SAXS/SANS and XAS analyses: impact on As binding. *Environ. Sci. Nano* **4**, 938–954.

Guieu C., Huang W. W., Martin J. M. and Yong Y. Y. (1996) Outflow of trace metals into the Laptev Sea by the Lena River. *Mar. Chem.* **53**, 255–267.

Guo L. A. and Santschi P. H. (2007) Ultrafiltration and its applications to sampling and characterisation of aquatic colloids. In *IUPAC Series on Analytical and Physical Chemistry of Environmental Systems*, vol. 10, p. 159.

Hassellöv M. and von der Kammer F. (2008) Iron oxides as geochemical nanovectors for metal transport in soil-river systems. *Elements* **4**, 401–406.

Hawkings J. R., Wadham J. L., Tranter M., Raiswell R., Benning L. G., Statham P. J., Tedstone A., Nienow P., Lee K. and Telling J. (2014) Ice sheets as a significant source of highly reactive nanoparticulate iron to the oceans. *Nat. Commun.* **5**, 3929.

Herndon E., AlBashaireh A., Singer D., Chowdhury T. R., Gu B. and Graham D. (2017) Influence of iron redox cycling on organo-mineral associations in Arctic tundra soil. *Geochim. Cosmochim. Acta* **207**, 210–231.

Hodson A., Nowak A., Sabacka M., Jungblut A., Navarro F., Pearce D., Ávila-Jiménez M. L., Convey P. and Vieira G. (2017) Climatically sensitive transfer of iron to maritime Antarctic ecosystems by surface runoff. *Nat. Commun.* **8**, 14499.

Huh Y. and Edmond J. M. (1999) The fluvial geochemistry of the rivers of Eastern Siberia: III. Tributaries of the Lena and Anbar draining the basement terrain of the Siberian Craton and the Trans-Baikal Highlands. *Geochim. Cosmochim. Acta* **63**, 967–987.

Huh Y., Panteleyev G., Babich D., Zaitsev A. and Edmond J. M. (1998) The fluvial geochemistry of the rivers of eastern Siberia: II. Tributaries of the Lena, Omoloy, Yana, Indigirka, Kolyma, and Anadry draining the collisional/accretionary zone of the Verkhoyansk and Cherskiy ranges. *Geochim. Cosmochim. Acta* **62**, 2053–2075.

Ilina S. M., Poitrasson F., Lapitskiy S. A., Alekhin Y. V., Viers J. and Pokrovsky O. S. (2013) Extreme iron isotope fractionation between colloids and particles of boreal and temperate organic-rich waters. *Geochim. Cosmochim. Acta* **101**, 96–111.

Ingri J., Malinovsky D., Rodushkin I., Baxter D. C., Widerlund A., Andersson P., Gustafsson Ö., Forsling W. and Öhlander B. (2006) Iron isotope fractionation in river colloidal matter. *Earth Planet. Sci. Lett.* **245**, 792–798.

Ingri J., Widerlund A., Land M., Gustafsson Ö., Andersson P. and Öhlander B. (2000) Temporal variations in the fractionation of the rare earth elements in a Boreal river; the role of colloidal particles. *Chem. Geol.* **166**, 23–45.

Jambor J. L. and Dutrizac J. E. (1998) Occurrence and constitution of natural and synthetic ferrihydrite, a widespread iron oxyhydroxide. *Chem. Rev.* **98**, 2549–2586.

Janney D. E., Cowley J. M. and Buseck P. R. (2000) Transmission electron microscopy of synthetic 2- and 6- line ferrihydrite. *Clays Clay Miner.* **48**, 111–119.

Karlsson T., Persson P., Skyllberg U., Mörth C.-M. and Giesler R. (2008) Characterization of Iron(III) in organic soils using extended X-ray absorption fine structure spectroscopy. *Environ. Sci. Technol.* **42**, 5449–5454.

Karlsson T. and Persson P. (2010) Coordination chemistry and hydrolysis of Fe(III) in a peat humic acid studied by X-ray absorption spectroscopy. *Geochim. Cosmochim. Acta* **74**, 30–40.

Karlsson T. and Persson P. (2012) Complexes with aquatic organic matter suppress hydrolysis and precipitation of Fe(III). *Chem. Geol.* **322–323**, 19–27.

Kopáček J., Klementová Š. and Norton S. A. (2005) Photochemical production of ionic and particulate aluminum and iron in lakes. *Environ. Sci. Technol.* **39**, 3656–3662.

Krachler R., Krachler R. F., Wallner G., Steier P., El Abiead Y., Wiesinger H., Jirsa F. and Keppler B. K. (2016) Sphagnum-dominated bog systems are highly effective yet variable sources of bio-available iron to marine waters. *Sci. Total Environ.* **556**, 53–62.

Kritzberg E. S., Villanueva A. B., Jung M. and Reader H. E. (2014) Importance of boreal rivers in providing iron to marine waters. *PLoS ONE* **9**.

Lalonde K., Mucci A., Ouellet A. and Gelinas Y. (2012) Preservation of organic matter in sediments promoted by iron. *Nature* **483**, 198–200.

Lam P. J. and Bishop J. K. B. (2008) The continental margin is a key source of iron to the HNLC North Pacific Ocean. *Geophys. Res. Lett.* **35**, 1–5.

Lerotic M., Mak R., Wirick S., Meirer F. and Jacobsen C. (2014) Mantis: a program for the analysis of x-ray spectromicroscopy data. *J. Synchrotron Radiat.* **21**, 1206–1212.

Leventhal J. and Taylor C. (1990) Comparison of methods to determine degree of pyritization. *Geochim. Cosmochim. Acta* **54**, 2621–2625.

Lindsay W. L. and Schwab A. P. (1982) The chemistry of iron in soils and its availability to plants. *J. Plant Nutr.* **5**, 821–840.

Liu B., Yang D., Ye B. and Berezovskaya S. (2005) Long-term open-water season stream temperature variations and changes over Lena River Basin in Siberia. *Glob. Planet. Change* **48**, 96–111.

Lofts S., Tipping E. and Hamilton-Taylor J. (2008) The chemical speciation of Fe(III) in freshwaters. *Aquat. Geochem.* **14**, 337–358.

Mann P. J., Davydova A., Zimov N., Spencer R. G. M., Davydov S., Bulygina E., Zimov S. and Holmes R. M. (2012) Controls on the composition and lability of dissolved organic matter in Siberia's Kolyma River basin. *J. Geophys. Res.: Biogeosci.* **1**, 117.

Mann P. J., Eglinton T. I., McIntyre C. P., Zimov N., Davydova A., Vonk J. E., Holmes R. M. and Spencer R. G. M. (2015) Utilization of ancient permafrost carbon in headwaters of Arctic fluvial networks. *Nat. commun.* **6**.

Martin J., Guan D., Elbaz-Poulichet F., Thomas A. and Gordeev V. (1993). *Preliminary assessment of the distributions of some trace elements (arsenic, cadmium, copper, iron, nickel, lead, iron, and zinc) in a pristine aquatic environment: The Lena River Estuary (Russia)* **43**, 185–199.

Martin J.-M. and Meybeck M. (1979) Elemental mass-balance of material carried by major world rivers. *Mar. Chem.* **7**, 173–206.

Mayer M. L. (1994) Surface area control of organic carbon accumulation in continental shelf sediments. *Geochim. Cosmochim. Acta* **58**, 1271–1284.

Neubauer E., Köhler S. J., Von Der Kammer F., Laudon H. and Hofmann T. (2013) Effect of pH and stream order on iron and arsenic speciation in boreal catchments. *Environ. Sci. Technol.* **47**, 7120–7128.

Oakes M., Weber R. J., Lai B., Russell A. and Ingall E. D. (2012) Characterization of iron speciation in urban and rural single particles using XANES spectroscopy and micro X-ray fluorescence measurements: investigating the relationship between speciation and fractional iron solubility. *Atmos. Chem. Phys.* **12**, 745–756.

Passow U. (2004) Switching perspectives: do mineral fluxes determine particulate organic carbon fluxes or vice versa? *Geochem. Geophys. Geosyst.* **5**, 1–5.

Perret D., Gaillard J. F., Dominik J. and Atteia O. (2000) The diversity of natural hydrous iron oxides. *Environ. Sci. Technol.* **34**, 3540–3546.

Peterson B. J., Holmes R. M., McClelland J. W., Vörösmarty C. J., Lammers R. B., Shiklomanov A. I., Shiklomanov I. A. and Rahmstorf S. (2002) Increasing river discharge to the Arctic Ocean. *Science* **298**, 2171–2173.

Pokrovsky O. S. and Schott J. (2002) Iron colloids/organic matter associated transport of major and trace elements in small boreal rivers and their estuaries (NW Russia). *Chem. Geol.* **190**, 141–179.

Pokrovsky O. S., Schott J. and Dupré B. (2006) Trace element fractionation and transport in boreal rivers and soil porewaters of permafrost-dominated basaltic terrain in Central Siberia. *Geochim. Cosmochim. Acta* **70**, 3239–3260.

Pokrovsky O. S., Viers J., Shirokova L. S., Shevchenko V. P., Filipov A. S. and Dupré B. (2010) Dissolved, suspended, and colloidal fluxes of organic carbon, major and trace elements in the Severnaya Dvina River and its tributary. *Chem. Geol.* **273**, 136–149.

Pokrovsky O. S., Shirokova L. S., Kirpotin S. N., Audry S., Viers J. and Dupré B. (2011) Effect of permafrost thawing on organic carbon and trace element colloidal speciation in the thermokarst lakes of western Siberia. *Biogeosciences* **8**, 565–583.

Pokrovsky O. S., Shirokova L. S., Viers J., Gordeev V. V., Shevchenko V. P., Chupakov A. V., Vorobieva T. Y., Candaudap F., Causserand C., Lanzanova A. and Zouiten C. (2014) Fate of colloids during estuarine mixing in the Arctic. *Ocean Sci.* **10**, 107–125.

Pokrovsky O. S., Manasypov R. M., Loiko S. V., Krickov I. A., Kopysov S. G., Kolesnichenko L. G., Vorobyev S. N. and Kirpotin S. N. (2016) Trace element transport in western Siberian rivers across a permafrost gradient. *Biogeosciences* **13**, 1877.

Poulton S. W. and Raiswell R. (2005) Chemical and physical characteristics of iron oxides in riverine and glacial meltwater sediments. *Chem. Geol.* **218**, 203–221.

Rachold V., Alabyan A., Hubberten H. W., Korotaev V. N. and Zaitsev A. A. (1996) Sediment transport to the Laptev

Sea – hydrology and geochemistry of the Lena River. *Polar Res.* **15**, 183–196.

Raiswell R. and Canfield D. E. (2012) The iron biogeochemical cycle past and present. *Geochem. Perspect.* **1**, 1–220.

Romanovsky V. E., Smith S. L. and Christiansen H. H. (2010) Permafrost thermal state in the polar northern hemisphere during the international polar year 2007–2009: a synthesis. *Permafr. Periglac. Process.* **21**, 106–116.

Rose J., Vilge A., Olivie-Lauquet G., Masion A., Frechou C. and Bottero J. Y. (1998) Iron speciation in natural organic matter colloids. *Colloids Surfaces A Physicochem. Eng. Asp.* **136**, 11–19.

Rouxel O. J., Bekker A. and Edwards K. J. (2005) Iron isotope constraints on the archean and Paleoproterozoic Ocean Redox State. *Science (80)* **307**, 1088–1091.

Salvadó J. A., Tesi T., Andersson A., Ingri J., Dudarev O. V., Semiletov I. P. and Gustafsson Ö. (2015) Organic carbon remobilized from thawing permafrost is resequestered by reactive iron on the Eurasian Arctic Shelf. *Geophys. Res. Lett.* **42**, 8122–8130.

Sánchez-García L., Alling V., Pugach S., Vonk J., Van Dongen B., Humborg C., Dudarev O., Semiletov I. and Gustafsson Ö. (2011) Inventories and behavior of particulate organic carbon in the Laptev and East Siberian seas. *Global Biogeochem. Cycles* **25**, 1–13.

Schroth A. W., Crusius J., Sholkovitz E. R. and Bostick B. C. (2009) Iron solubility driven by speciation in dust sources to the ocean. *Nat. Geosci.* **2**, 337–340.

Schroth A. W., Crusius J., Chever F., Bostick B. C. and Rouxel O. J. (2011) Glacial influence on the geochemistry of riverine iron fluxes to the Gulf of Alaska and effects of deglaciation. *Geophys. Res. Lett.* **38**, 1–6.

Schwertmann U., Fitzpatrick R. W., Taylor R. M. and Lewis D. G. (1979) The influence of aluminum on iron oxides. Part I. preparation and properties of A1-substituted hematites. *Clays Clay Miner.* **27**, 105–112.

Schwertmann U. and Murad E. (1983) Effect of pH on the formation of goethite and hematite from ferrihydrite. *Clays Clay Miner.* **31**, 277–284.

Schwertmann U., Wagner F. and Knicker H. (2005) Ferrihydrite-humic associations. *Soil Sci. Soc. Am. J.* **69**, 1009.

Severmann S., Johnson C. M., Beard B. L. and McManus J. (2006) The effect of early diagenesis on the Fe isotope compositions of porewaters and authigenic minerals in continental margin sediments. *Geochim. Cosmochim. Acta* **70**, 2006–2022.

Severmann S., McManus J., Berelson W. M. and Hammond D. E. (2010) The continental shelf benthic iron flux and its isotope composition. *Geochim. Cosmochim. Acta* **74**, 3984–4004.

Sharoglazov A. S. (1965) Resources of surface waters of the USSR (1965). *Lena – Indigirka district, Izd-vo Gidrometeorologich-eskoe* **17**, 119 (in Russian).

Sharoglazov A. S. (1967) Resources of surface waters of the USSR (1967). *Lena – Indigirka district, Leningrad, Gidrometeoizdat* **17**, 649 (in Russian).

Shields M. R., Bianchi T. S., Gélinas Y., Allison M. A. and Twilley R. R. (2016) Enhanced terrestrial carbon preservation promoted by reactive iron in deltaic sediments. *Geophys. Res. Lett.* **43**, 1149–1157.

Sholkovitz E. R. (1976) Flocculation of dissolved organic and inorganic matter during the mixing of river water and seawater. *Geochim. Cosmochim. Acta* **40**, 831–845.

Sjöstedt C., Persson I., Hesterberg D., Kleja D. B., Borg H. and Gustafsson J. P. (2013) Iron speciation in soft-water lakes and soils as determined by EXAFS spectroscopy and geochemical modelling. *Geochim. Cosmochim. Acta* **105**, 172–186.

Soltis J. A., Feinberg J. M., Gilbert B. and Penn R. L. (2016) Phase transformation and particle-mediated growth in the formation of hematite from 2-line ferrihydrite. *Cryst. Growth Des.* **16**, 922–932.

Spencer R. G., Mann P. J., Dittmar T., Eglinton T. I., McIntyre C., Holmes R. M., Zimov N. and Stubbins A. (2015) Detecting the signature of permafrost thaw in Arctic rivers. *Geophys. Res. Lett.* **42**, 2830–2835.

Stolbovoi V. and McCallum I. (2002) *CD-ROM Land Resources of Russia* edited. International Institute for Applied Systems Analysis and the Russian Academy of Science, Laxenburg, Austria.

Stolpe B., Guo L. and Shiller A. M. (2013) Binding and transport of rare earth elements by organic and iron-rich nanocolloids in alaskan rivers, as revealed by field-flow fractionation and ICP-MS. *Geochim. Cosmochim. Acta* **106**, 446–462.

Striegl R. G., Aiken G. R., Dornblaser M. M., Raymond P. A. and Wickland K. P. (2005) A decrease in discharge-normalized DOC export by the Yukon River during summer through autumn. *Geophys. Res. Lett.* **32**, 1–4.

Stumm W. and Morgan J. J. (1996) *Aquatic Chemistry: Chemical Equilibria and Rates in Natural Waters (Environ. Sci. Technol)*. Wiley.

Sundman A., Karlsson T., Laudon H. and Persson P. (2014) XAS study of iron speciation in soils and waters from a boreal catchment. *Chem. Geol.* **364**, 93–102.

Tagliabue A., Bowie A. R., Philip W., Buck K. N., Johnson K. S. and Saito M. A. (2017) The integral role of iron in ocean biogeochemistry. *Nature* **543**.

Tamocai C., Canadell J. G., Schuur E. A. G., Kuhry P., Mazhitova G. and Zimov S. (2009) Soil organic carbon pools in the northern circumpolar permafrost region. *Global Biogeochem. Cycles* **23**, 1–11.

Taylor S. R. and McLennan S. M. (1985) *The continental crust: its composition and evolution*.

Tesi T., Semiletov I., Dudarev O., Andersson A. and Gustafsson Ö. (2016) Matrix association effects on hydrodynamic sorting and degradation of terrestrial organic matter during cross-shelf transport in the Laptev and East Siberian shelf seas. *J. Geophys. Res. G Biogeosci.* **121**, 731–752.

Toner B. M., Santelli C. M., Marcus M. A., Wirth R., Chan C. S., McCollom T., Bach W. and Edwards K. J. (2009) Biogenic iron oxyhydroxide formation at mid-ocean ridge hydrothermal vents: Juan de Fuca Ridge. *Geochim. Cosmochim. Acta* **73**, 388–403.

Van Schaik J. W. J., Persson I., Kleja D. B. and Gustafsson J. P. (2008) EXAFS study on the reactions between iron and fulvic acid in acid aqueous solutions. *Environ. Sci. Technol.* **42**, 2367–2373.

Vasyukova E. V., Pokrovsky O. S., Viers J., Oliva P., Dupré B., Martin F. and Candaudap F. (2010) Trace elements in organic- and iron-rich surficial fluids of the boreal zone: assessing colloidal forms via dialysis and ultrafiltration. *Geochim. Cosmochim. Acta* **74**, 449–468.

Vasyukova E., Pokrovsky O. S., Viers J. and Dupré B. (2012) New operational method of testing colloid complexation with metals in natural waters. *Appl. Geochem.* **27**, 1226–1237.

Vonk J. E., Mann P. J., Davydov S., Davydova A., Spencer R. G. M., Schade J., Sobczak W. V., Zimov N., Zimov S., Bulygina E., Eglinton T. I. and Holmes R. M. (2013) High biolability of ancient permafrost carbon upon thaw. *Geophys. Res. Lett.* **40**, 2689–2693.

Von der Heyden B. P., Roychoudhury A. N., Mtshali T. N., Tyliszczak T. and Myneni S. C. B. (2012) Chemically and geographically distinct solid-phase iron pools in the Southern Ocean. *Science* **338**, 1199–1201.

Von der Heyden B. P., Hauser E. J., Mishra B., Martinez G. A., Bowie A. R., Tyliszczak T., Mtshali T. N., Roychoudhury A. N. and Myneni S. C. (2014) Ubiquitous presence of Fe (II) in aquatic colloids and its association with organic carbon. *Environ. Sci. Technol. Lett.* **1**, 387–392.

Wiederhold J. G., Teutsch N., Kraemer S. M., Halliday A. N. and Kretzschmar R. (2007) Iron isotope fractionation in oxic soils by mineral weathering and podzolization. *Geochim. Cosmochim. Acta* **71**, 5821–5833.

Yang D., Kane D. L., Hinzman L. D., Zhang X., Zhang T. and Ye H. (2002) Siberian Lena River hydrologic regime and recent change. *J. Geophys. Res. Atmos.* **107**, 1–10.

Yee N., Shaw S., Benning L. G. and Nguyen T. H. (2006) The rate of ferrihydrite transformation to goethite via the Fe(II) pathway. *Am. Mineral.* **91**, 92–96.

Zhang T. (2005) Influence of seasonal snow cover on the ground thermal regime: an overview. *Rev. Geophys.* **43**, RG4002.

Zhao J. M., Huggins F. E., Feng Z. and Huffman G. P. (1994) Ferrihydrite – surface structure and its effects on phase-transformation. *Clays Clay Miner.* **42**, 737–746.

Associate editor: Timothy J. Shaw